1995

Distribution of the bottom-simulating reflector in the offshore Taiwan collision zone : implications for fluid migration

Wu-Cheng Chi
San Jose State University

DISTRIBUTION OF THE BOTTOM-SIMULATING REFLECTOR IN THE OFFSHORE TAIWAN COLLISION ZONE: IMPLICATIONS FOR FLUID MIGRATION

A Thesis

Presented to

The Faculty of the Department of Geology

San Jose State University

In Partial Fulfillment

of the Requirements for the Degree

Master of Science

by

Wu-Cheng Chi

May 1995

APPROVED FOR THE DEPARTMENT OF GEOLOGY

Dr. Donald Reed

Dr. David Andersen

Dr. Richard Sedlock

APPROVED FOR THE UNIVERSITY

ABSTRACT

DISTRIBUTION OF THE BOTTOM-SIMULATING REFLECTOR IN THE OFFSHORE TAIWAN COLLISION ZONE: IMPLICATIONS FOR FLUID MIGRATION

by Wu-Cheng Chi

The distribution and sub-bottom depth of the bottom-simulating reflector (BSR) in the offshore Taiwan accretionary prism were mapped using migrated 6-channel reflection profiles. The BSR sub-bottom depth (two-way traveltime) increases with increasing water depth, suggesting that the BSR marks the base of the methane hydrate stability field. A "flat spot" was found under the BSR, suggesting that the hydrate-filled pore-space causes lower permeability, therefore enhancing the entrapment of free gas. The BSR is located in sediments derived from the Taiwan orogen and offscraped strata of the Chinese continental margin, which may have high amounts of organic carbon, and therefore may be the source of the methane. The BSR sub-bottom depth decreases near several fault zones and beneath mud volcanoes, possibly due to variations in heat flow related to focused fluid flow. The BSR sub-bottom depth was used to estimate geothermal gradient, ranging from 17 to 160 °C/km and increasing toward the toe of the prism. These observations may be related to extensive sediment dewatering, fluid migration and sediment blanketing.

ACKNOWLEDGEMENT

I need to thank my advisor, Don Reed, for his efforts in educating me. He provides a good atmosphere for students to study. Thanks should also be given to Dennis Fox, who helped me learn many computer skills. Justin Hirtzel is thanked for inviting me to see a moon eclipse on the top floor of Duncan Hall during a "very cold" winter night. I feel at home working in this group. I thank Richard Sedlock and Dave Andersen; their comments greatly improved this paper. I also thank Prof. Char-shine Liu at National Taiwan University for giving me a chance to work with him while I was in Taipei.

It is hard to image that I am studying at a place 6000 miles away from home. I could not have done it without my family's support, especially my Mom. I am lucky enough to get married with Ching-Yen. She brings many wonderful things to me.

TABLE OF CONTENTS

	Page
ABSTRACT	iv
INTRODUCTION	1
PREVIOUS STUDIES OF GAS HYDRATES AND BSRS	5
Properties of Gas Hydrates	5
Characteristics of BSRs	7
Seismic Modeling of BSRs	7
Results of Deep Sea Drilling Project and Ocean Drilling Program	8
GEOLOGIC SETTING OF TAIWAN COLLISION	10
METHODS AND RESULTS	14
DISCUSSION	29
Sediment Types and Distribution of BSRs	29
Implications of BSR Sub-bottom Depth	31
BSR Depth as Evidence of Fluid Migration	34
A Model of Geothermal Gradient in Offshore Taiwan Accretionary Prism	35
Dewatering near the Toe of the Accretionary Prism	37
Low Geothermal Gradient near the Boundary of Upper and Lower Slope Domains	39

Possible Heat Flow Value Range 41

CONCLUSIONS 42

REFERENCES CITED 43

List of Illustrations

Page

Figure 1. Example of BSR 2

Figure 2. Hydrate Stability Data Compiled from Laboratory Data and Field Observation 3

Figure 3. Stable Hydrate Zone under the Ocean 6

Figure 4. Taiwan Location Map 11

Figure 5. Tectonic Framework of Offshore Southern Taiwan 12

Figure 6. Cross Sections of Taiwan Accretionary Prism 13

Figure 7. Tracks of 1990 6-channel Seismic Data 15

Figure 8a. Distribution of the Clear Type (Q1) BSRs 16

Figure 8b. Distribution of the Probable Type (Q2) BSRs 17

Figure 8c. Distribution of the Possible Type (Q3) BSRs 18

Figure 9. BSR Sub-bottom Depth Increases as Water Depth Increases 19

Figure 10. BSR Shallows Toward a Fault Zone 20

Figure 11. BSR Shallows Beneath a Mud Volcano 21

Figure 12. Contour Map of BSR Sub-bottom Depth 22

Figure 13a. Q1 type BSR Sub-bottom Depth vs. Water Depth 23

Figure 13b. Q2 type BSR Sub-bottom Depth vs. Water Depth 24

Figure 13c. Q3 type BSR Sub-bottom Depth vs. Water Depth 25

Figure 14a. Distribution of BSRs with Shallower-than-expected Sub-bottom Depth 27

Figure 14b. Distribution of BSRs with Deeper-than-expected Sub-bottom Depth 28

Figure 15. Direct Hydrocarbon Indicator Underneath the BSR 30

Figure 16. Variations of BSR Sub-bottom Depth in Area with Tight Curvature of Seafloor Topography 33

Figure 17. Contour Map of Estimated Geothermal Gradient 38

Figure 18. Structural Map of Study Area 40

INTRODUCTION

A bottom-simulating reflector, or BSR (Fig. 1), is a seismic reflector subparallel to the topography of the sea floor, and in some places it cuts across reflectors generated by sediment layers (Shipley and others, 1979). BSRs commonly are observed in continental slope sediments, particularly those associated with accretionary prisms (Hyndman and Davis, 1992). These seismic reflectors are generated by the acoustic impedance contrast at the base of a sediment layer containing methane hydrate (Shipley and others, 1979; Miller and others, 1991).

Methane hydrates are "ice-like" clathrate structures in which methane molecules are enclosed within a solid lattice of water molecules. Hydrates have been found in deep ocean sediments where there is a sufficient supply of methane and where pressure and temperature ranges between 0.2-5 MPa and 0-25 °C, respectively. The increase in temperature with depth below the seafloor causes methane hydrate to become unstable and decompose, despite increasing pressure. As a result, the base of the methane hydrate defines a "phase boundary" that separates the stable gas hydrate above from a field of instability below. The temperature at the BSR can be inferred from hydrate phase equilibria (Fig. 2) and estimated in-situ pressures. By converting the two-way traveltime of the BSR to depth and assuming a temperature at the sea floor, the regional geothermal gradient and heat flow can be estimated using the equation:

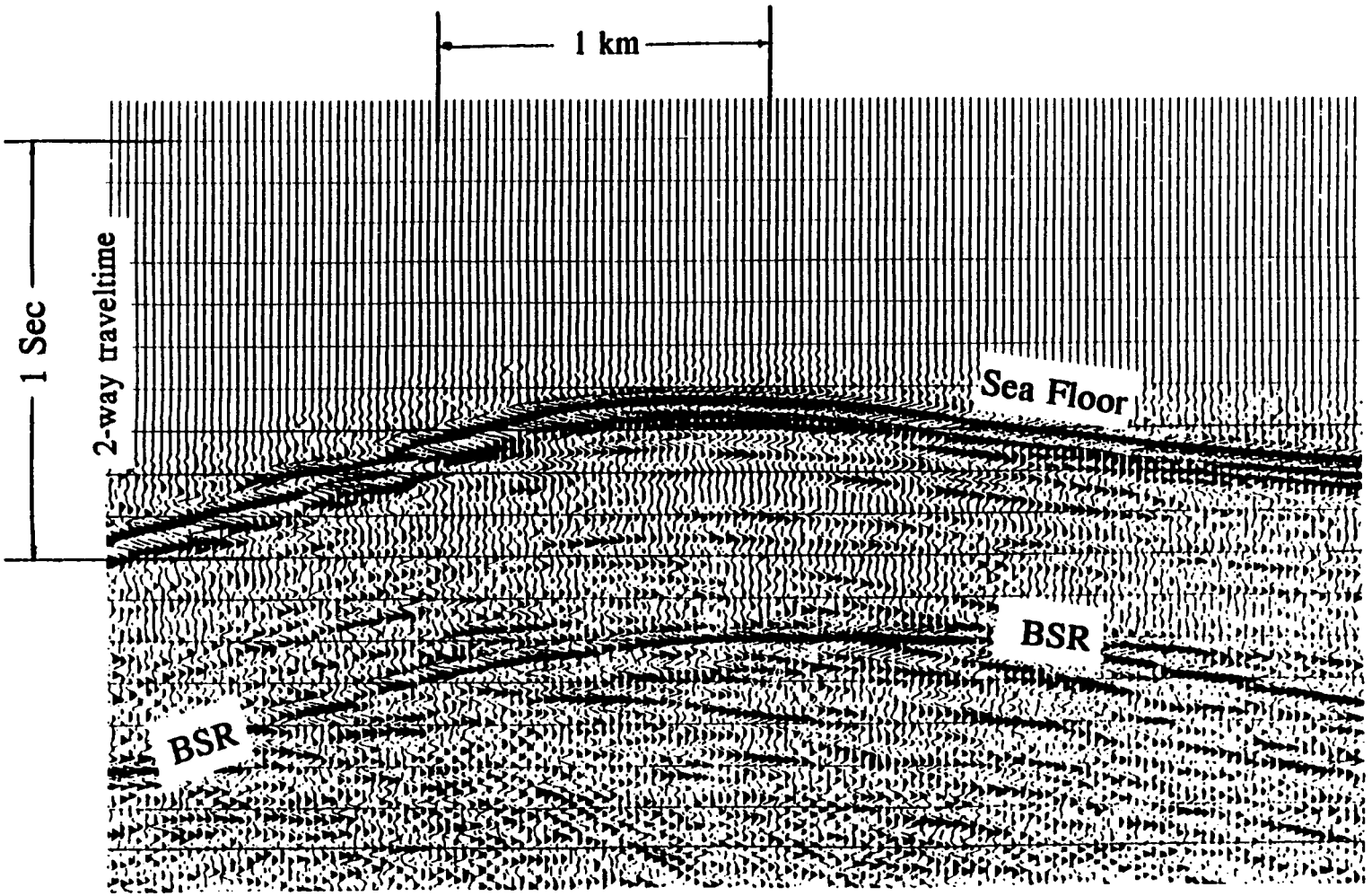

Figure 1. Example of BSR with Reversed Polarity Reflection located in anticlinal ridge.

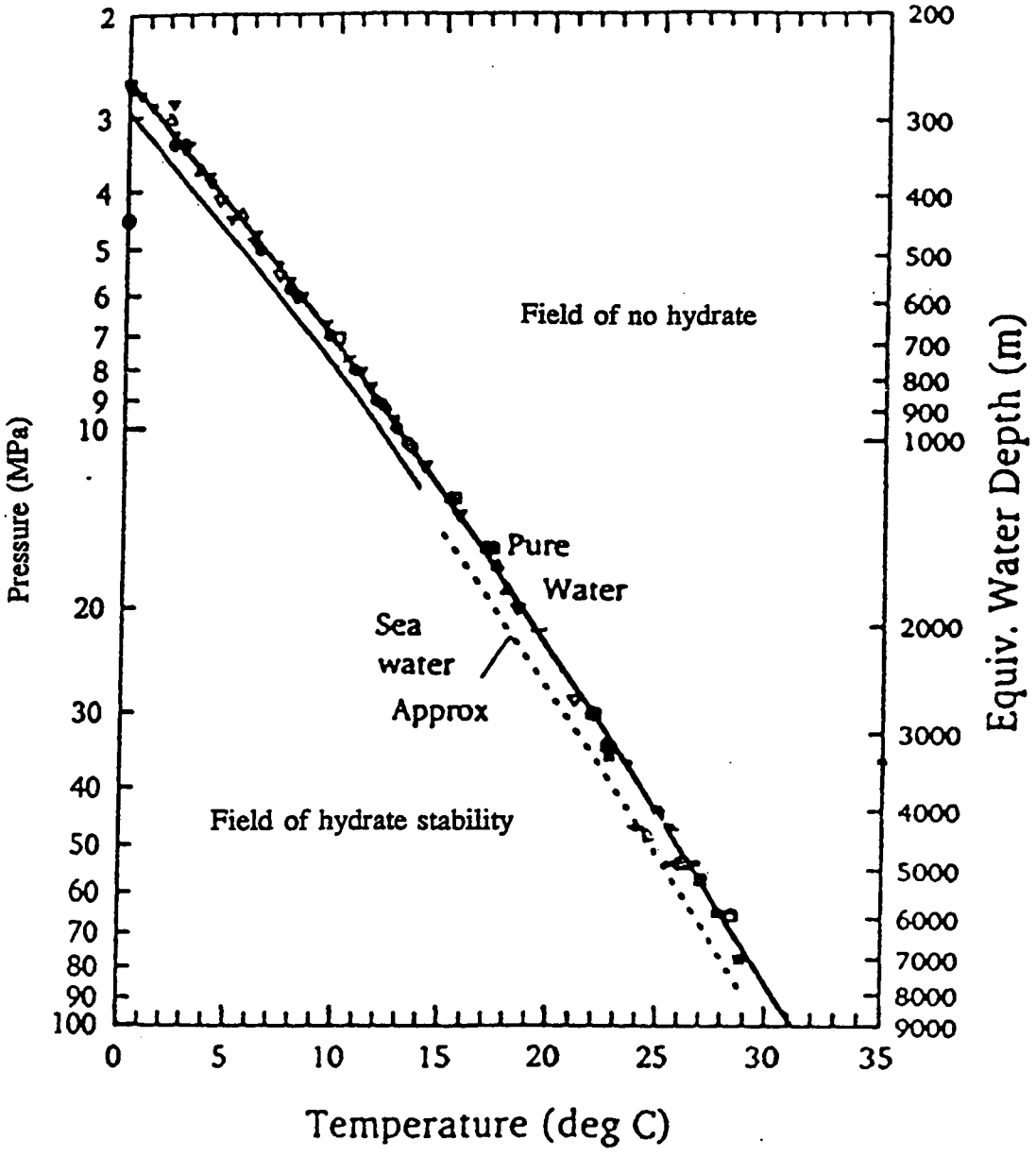

Figure 2. Hydrate stability data compiled from labortory data and field observation (redrawn from Hydman and others, 1992).

$Q = -k\ dt/dz$

Where Q: Heat flow, in mW/m^2

k: sediment thermal conductivity, in W/mK

dt/dz: geothermal gradient , in °C/km

t: temperature, in °C

z: sub-bottom depth, in km

This technique has been used to estimate heat flow in several accretionary prism settings (e.g., Hyndman and others, 1992; Yamono and others, 1992; Ashi and Taira, 1993; Zwart and Moore, 1993).

The distribution of the BSR in the offshore Taiwan accretionary prism was studied using migrated 6-channel reflection profiles. The BSR is widespread in the region of the collision zone. Water depths and the BSR sub-bottom depths were compiled across the accretionary prism, both in the region of subduction and that of collision. Using velocity-depth relations published in Hamilton (1980), travel-time measurements were converted to depth in meters. Variations in geothermal gradient, as inferred from variations in BSR sub-bottom depth, were used to study the thermal structures of the offshore Taiwan accretionary prism and were inferred as indicators of fluid flow during sediment dewatering with sediment offscraping.

PREVIOUS STUDIES OF GAS HYDRATES AND BSRS

Properties of Gas Hydrates

Methane hydrate-bearing sediments have physical and chemical properties different from either water- or gas-saturated sediments. Drilling and submersible diving studies have shown that methane hydrate can occur as a solid mass, fracture-filling vein, thin lens in sediment, or as a lobed mound (Rowe and Gettrust, 1993; Guinasso and others, 1994).

Methane in ocean sediment is biogenic or thermogenic origin; these sources can be differentiated by the CH_4/C_2H_6 ratio (Gamo and others, 1992). Higher CH_4/C_2H_6 ratios indicate a biogenic source related to bacterial reduction of organic carbon, which may be the common case in accretionary prisms (e.g., Gamo and others, 1992; Hyndman and Davis, 1993; Kvenvolden, 1993). Consequently, two-component (methane and water) phase equilibria (Fig. 2) have been used to estimate P-T conditions at the base of the methane hydrate zone.

The base of the methane hydrate zone represents the "phase boundary" that separates sediment with hydrate above from the sediment with gas or fluid below (Fig. 3). The higher rigidity of frozen hydrated sediment produces higher velocities ranging from 1.6 to 3.8 km/s, which are higher than velocities of sediment without hydrate (Shipley and Didyk, 1982; Rowe and Gettrust, 1993). The contrast in velocities at this boundary creates a reflector that commonly cuts across bedding plane reflections.

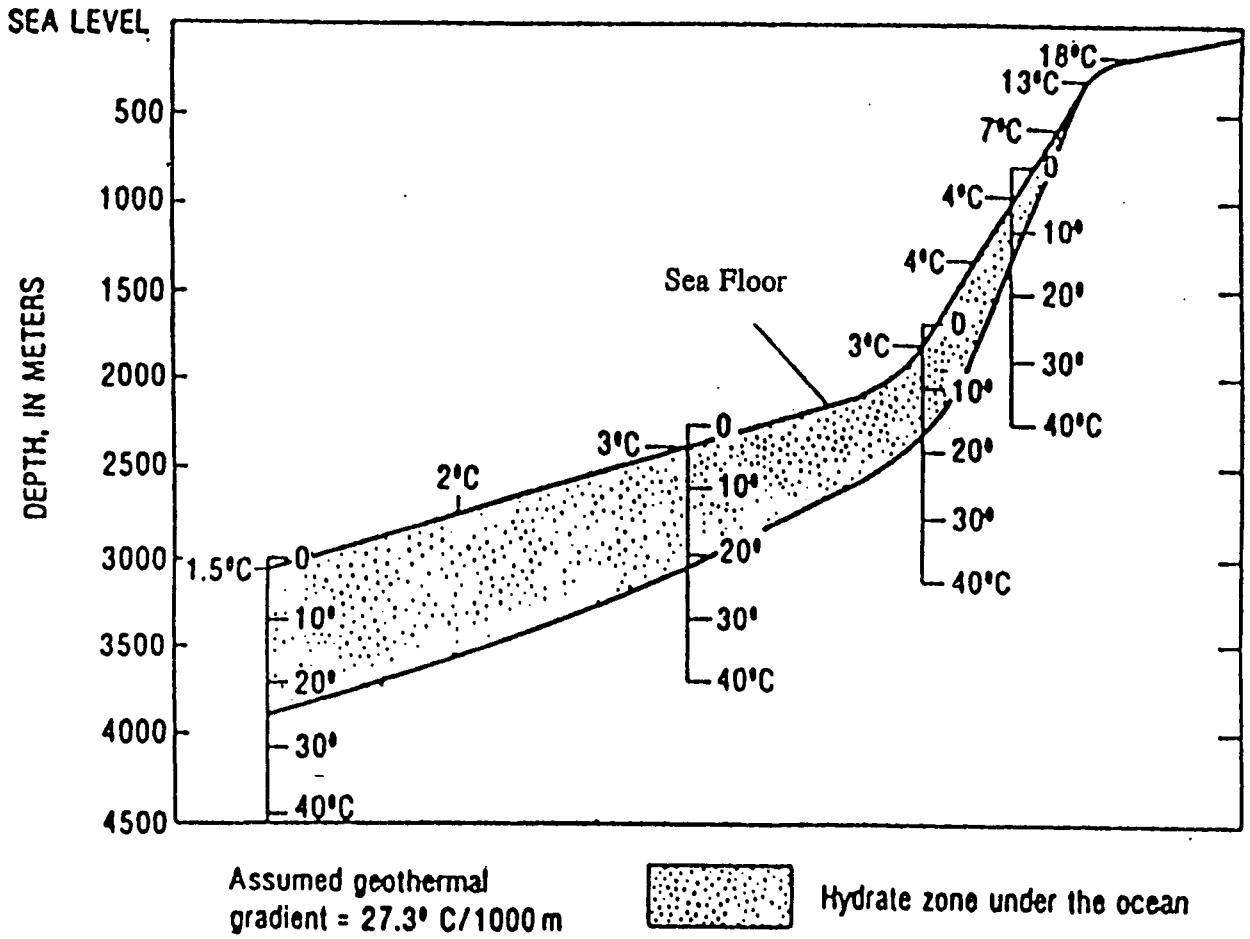

Figure 3. Stable Hydrate Zone under the ocean. Note the increasing BSR sub-bottom depth as water depth increases (redrawn from Kvenvolden and McDonald, 1985).

Characteristics of BSRs

According to Hyndman and Spence (1992), BSRs have the following seismic reflection characteristics (Fig. 1):

(1) The reflection polarity is reversed relative to the seafloor reflection, showing a decrease in acoustic impedance (product of velocity and density) across the boundary.

(2) The reflection coefficients are large, up to 50% of that of the sea floor, where:

$R = (d_2V_2 - d_1V_1)/(d_2V_2 + d_1V_1)$

R: reflection coefficient

d_1, d_2 : densities of the upper and lower media, respectively, in g/cm^3

V_1 ,V_2 : velocities of the upper and lower media, respectively, in m/sec.

(3) The BSR reflection usually is a single symmetrical pulse characteristic of a simple interface.

In addition, BSRs usually are several hundred meters beneath the sea floor and marked by a topography-parallel reflection, hence the designation "bottom-simulating reflector."

Seismic Modeling of BSRs

Many seismic modeling studies have suggested the presence of free gas below BSRs

(Miller and others, 1991; Bangs and others, 1993; Singh and others, 1993). The hydrate infilling of pore space of surface sediments can elevate seismic velocities, although vertical seismic profiles (VSPs) in Cascadia accretionary prism show only a slight velocity anomaly, suggesting that less than 10% of the pore space is filled with hydrate (MacKay and others, 1994). In addition, a layer of lower-than-expected sediment velocity below the BSR implies the presence of a few percent (by volume) free gas, which may dramatically reduce the seismic velocity of sediments. In other words, the velocity decrease due to gas below the hydrate could be the main factor contributing to the high seismic amplitude typical of BSRs. Miller and others (1991) analyzed seismic data from offshore Peru and suggested that high-amplitude BSRs are underlain by a layer more than 5.5 m thick of sediment and free gas, whereas the low-amplitude BSRs in their data are associated with a sediment-gas layer less than 5.5 m thick.

Results of Deep Sea Drilling Project and Ocean Drilling Program

The Deep Sea Drilling Project (DSDP) and Ocean Drilling Program (ODP) have provided valuable evidence for the presence of methane hydrate in marine sediments and have shown good agreement between the BSR sub-bottom depth and phase boundary conditions of methane hydrate. DSDP Leg 66 sampled sediments with very high gas/water ratios, strongly suggesting the decomposition of methane hydrate along offshore Mexico and Guatemala (Shipley and Didyk, 1982). A similar observation was made during Leg 84 offshore of Costa Rica (Kvenvolden and McDonald, 1983). Leg 76 on the Blake Outer

Ridge confirmed the presence of methane hydrates along eastern U.S. continental slope (Kvenvolden and Barnard, 1983). The latter two studies showed that methane in these areas is biogenic in origin (Kvenvolden and Barnard, 1983; Kvenvolden and McDonald, 1983).

A recent study during ODP Leg 131 on the Nankai accretionary prism showed that the sub-bottom temperatures estimated from the BSR depth correspond closely to the temperature and pressure for the decomposition of pure water-pure methane hydrate system under laboratory conditions (Hyndman and others, 1992). Pore-water geochemical studies on ODP Leg 141 suggested that hydrate occupies only a small fraction of the available pore space above the BSR (Froelich and others, 1993). ODP Leg 146 at the Cascade margin recovered methane hydrate and provided important evidence of free gas existing below the depth of the BSR (ODP Leg 146 Scientific Party, 1993).

GEOLOGIC SETTING OF TAIWAN COLLISION

Taiwan (Fig. 4) is located on the boundary between the Eurasian plate and Philippine Sea plate. Oceanic lithosphere of the South China Sea is subducting eastward beneath the Philippine Sea plate, resulting in the formation of the Manila Trench, the offshore Taiwan accretionary prism, forearc basin of the North Luzon Trough, and the Luzon volcanic arc (Fig. 5). Oceanic crust in the South China Sea in this area may be as old as 32 Ma, as inferred from marine magnetic anomalies (Tayor and Hayes, 1980). To the north, subduction changes into an arc-continent collision where the Chinese continental margin enters the subduction zone (Suppe, 1981). Although the timing of initial collision is still under debate, it probably began in the late middle Miocene (Teng, 1990) and is currently propagating southward (Suppe, 1984).

The submarine accretionary prism contains three distinct structural domains (Reed and others, 1992, Fig. 6): (1) a lower slope domain composed of mostly west-vergent ramp anticlines; (2) an upper slope domain with highly discontinuous reflections, suggesting intense deformation and, possibly, out-of-sequence thrusting and underplating; and (3) a backthrust domain located along the rear of the prism. The North Luzon Trough, a forearc basin, is truncated by the juxtaposition of the rear of the prism and the volcanic arc along backthrusts in the region of collision.

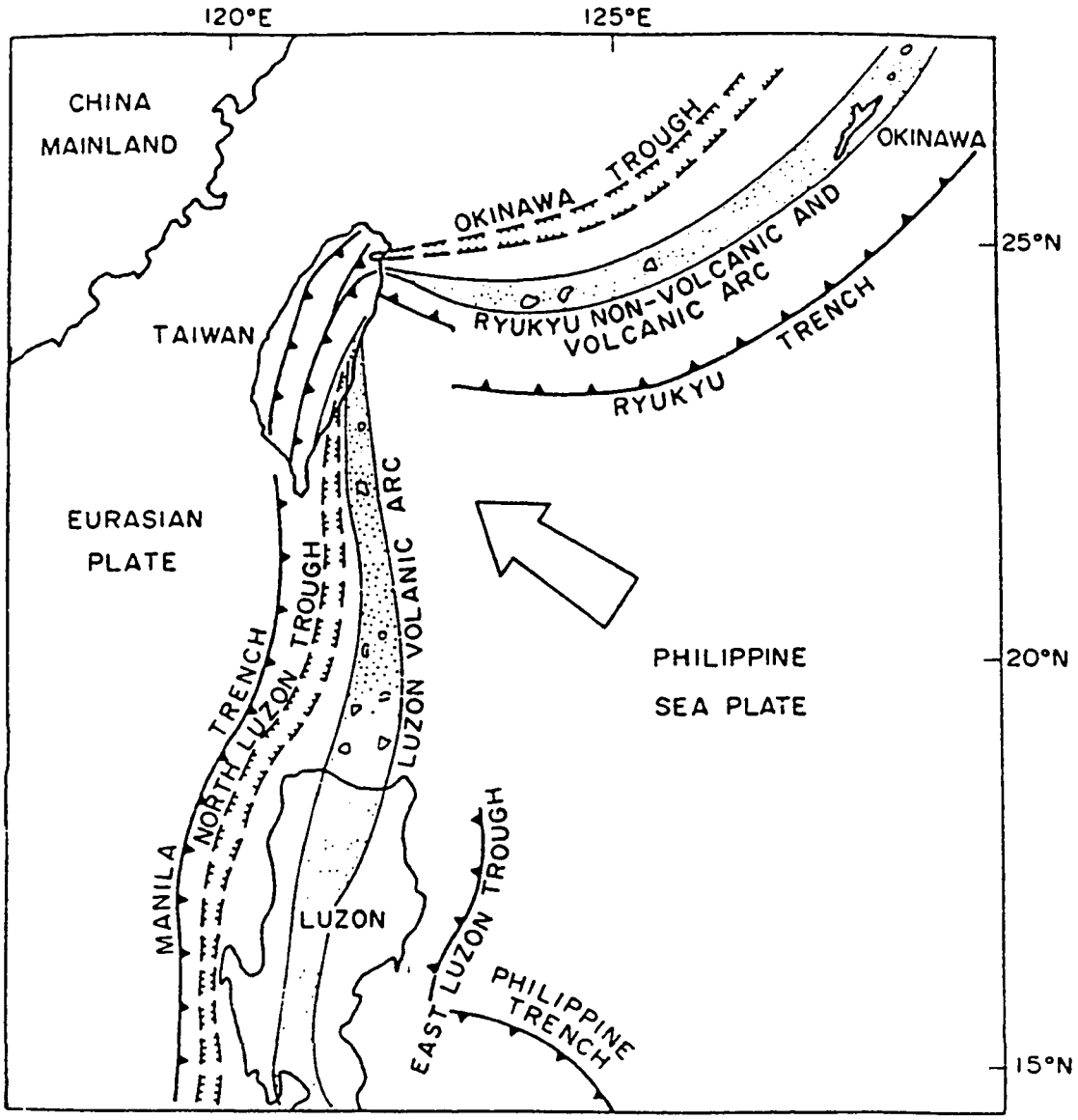

Figure 4. Taiwan location map (after Ho, 1986).

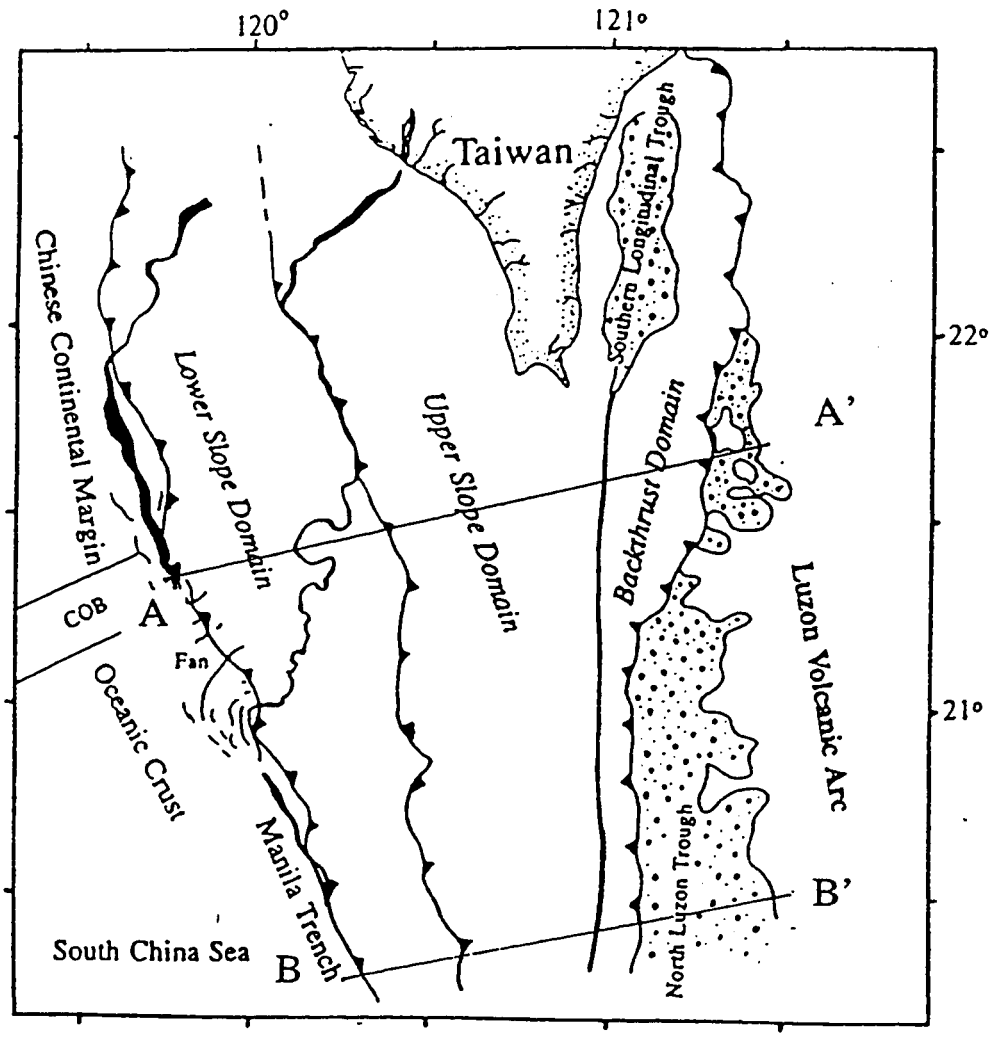

Figure 5. Tectonic framework of offshore southern Taiwan (after Reed and others, 1992). COB: Continent-ocean boundary.

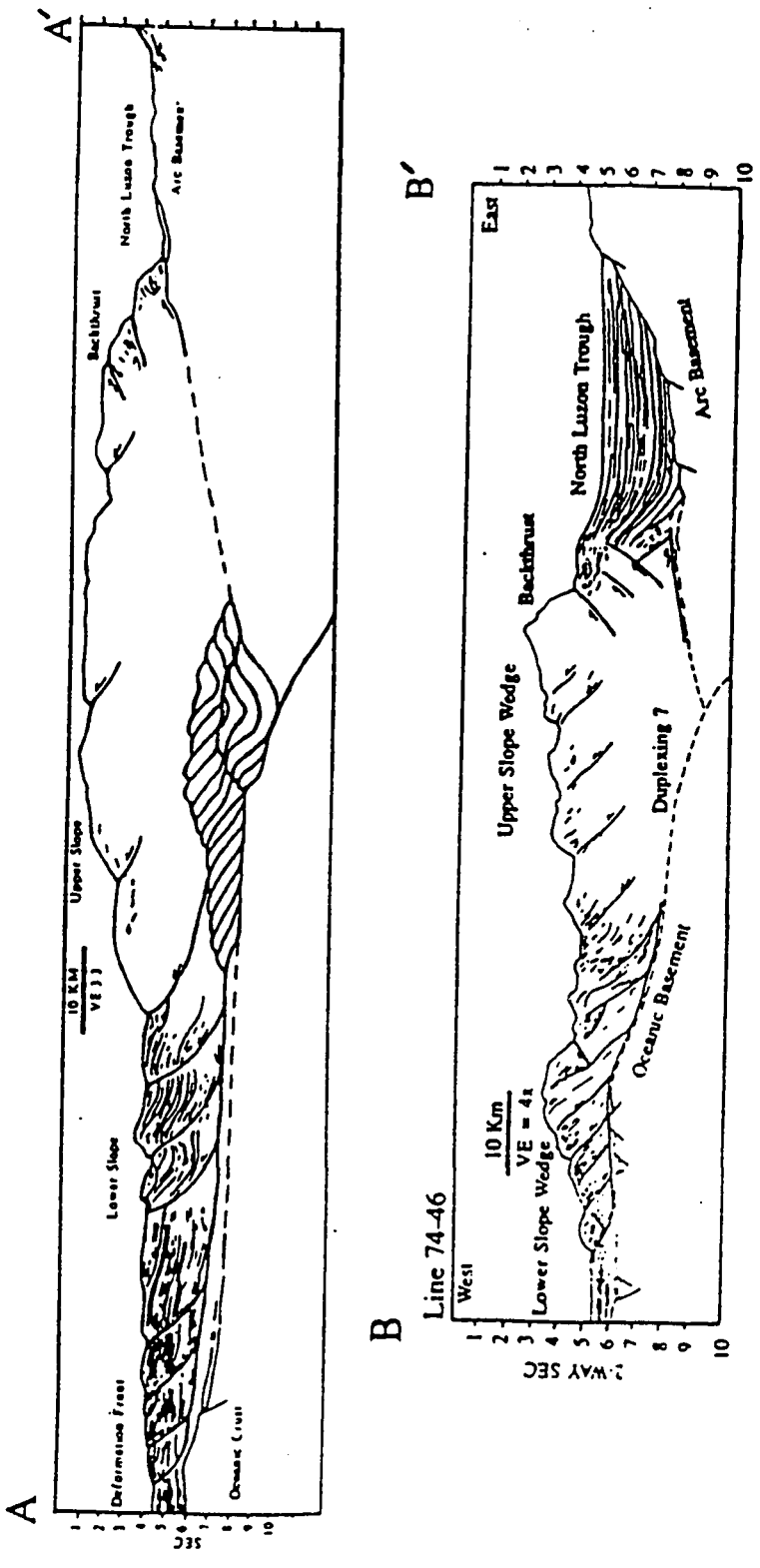

Figure 6. Cross sections of Taiwan accretionary prism (after Reed and others, 1992). Locations of sections shown on Figure 5.

METHODS AND RESULTS

This study is based on data acquired during a marine geophysical survey (Fig. 7) conducted in 1990 aboard the R/V Moana Wave of the University of Hawaii. More than 8000 kilometers of seismic reflection profiles were examined covering a region of 45,000 km^2. The BSR was measured at nearly 1,500 locations along the survey lines. These data were converted into methane hydrate distribution maps showing varying degrees of confidence in the accuracy of BSR identification (Fig. 8a, 8b, 8c). These maps show widespread occurrence of BSRs within the collision zone and the lower slope domain, where sediments derived from the Chinese continental margin and Taiwan orogen are offscraped along the deformation front. BSRs were commonly observed in hinge zones of anticlines, but were conspicuously absent beneath submarine canyons in the region.

The BSR sub-bottom depth generally increases with increasing water depth (Fig. 9). However, BSR depths decrease locally at several fault zones (Fig. 10) and beneath mud volcanoes (Fig. 11). In addition, a two-way traveltime contour map of the BSR sub-bottom depth(Fig. 12) shows a general shallowing of the BSR toward the toe of the accretionary prism, despite the increasing water depth. BSR sub-bottom depth also decreases where the Chinese continent enters the subduction zone, although water depths decrease in the region as well.

Several water depth vs. BSR sub-bottom depth plots were constructed (Fig. 13). The

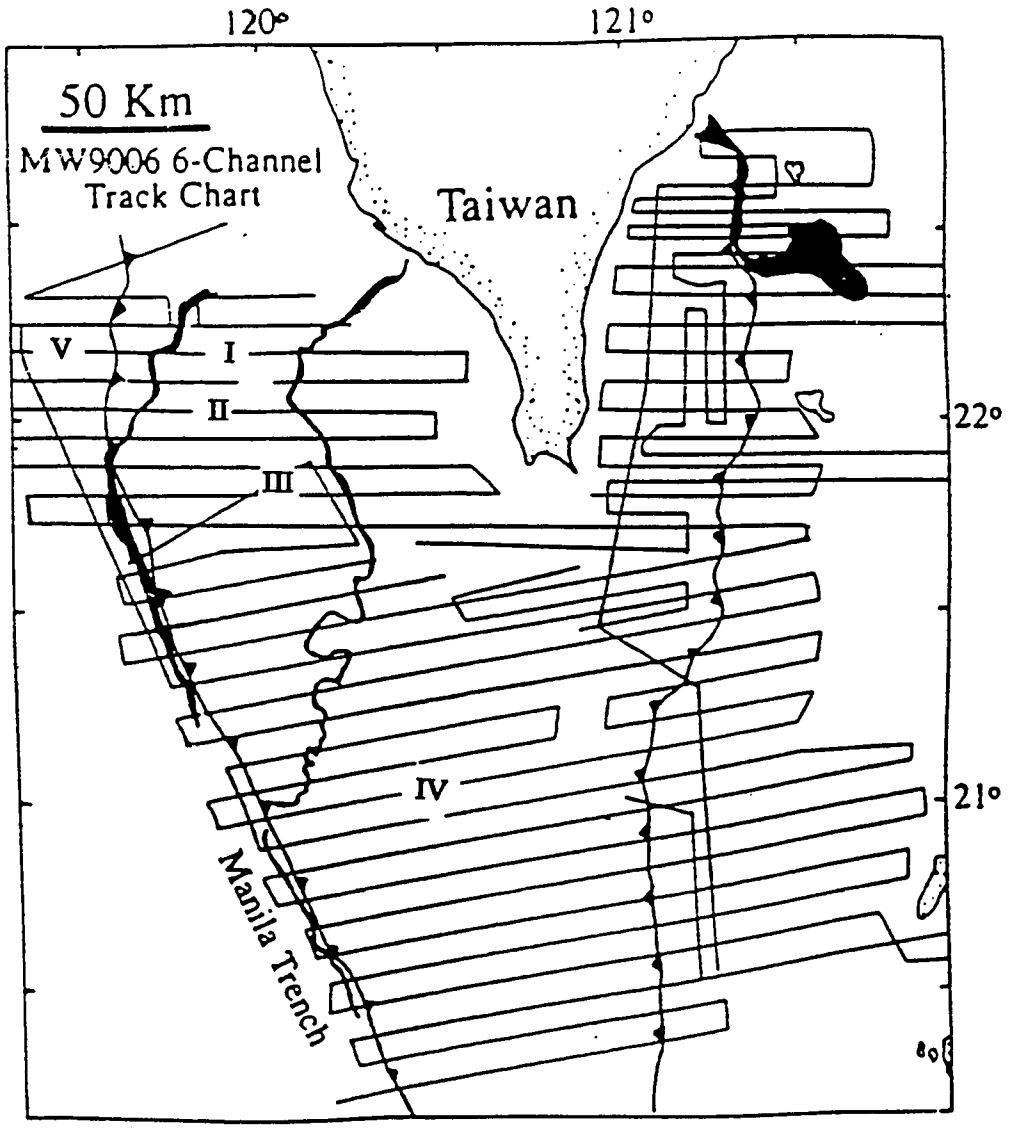

Figure 7. Tracks of 1990 6-channel Seismic Data (after Reed and others, 1992). Roman numerals as locations of illustrated profiles.

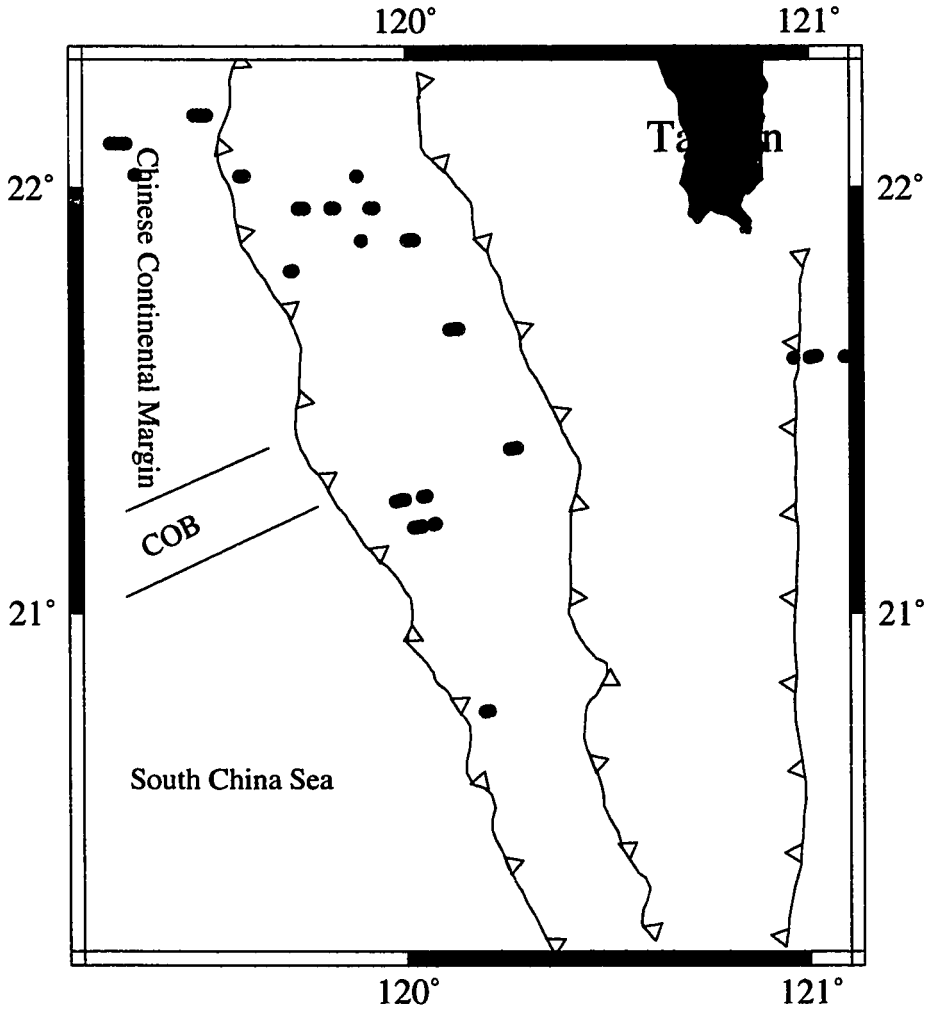

Figure 8a: Distribution of the clear type (Q1) BSRs.

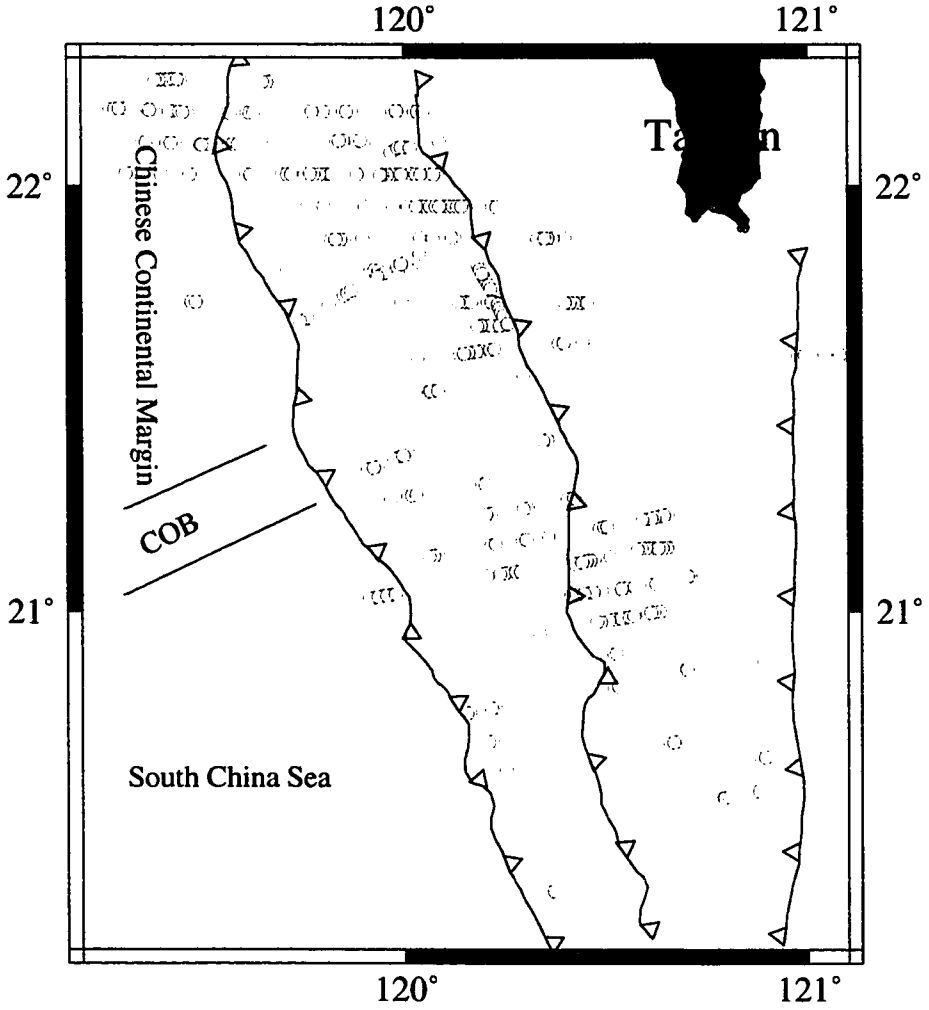

Figure 8b: Distribution of the probable type (Q2) BSRs.

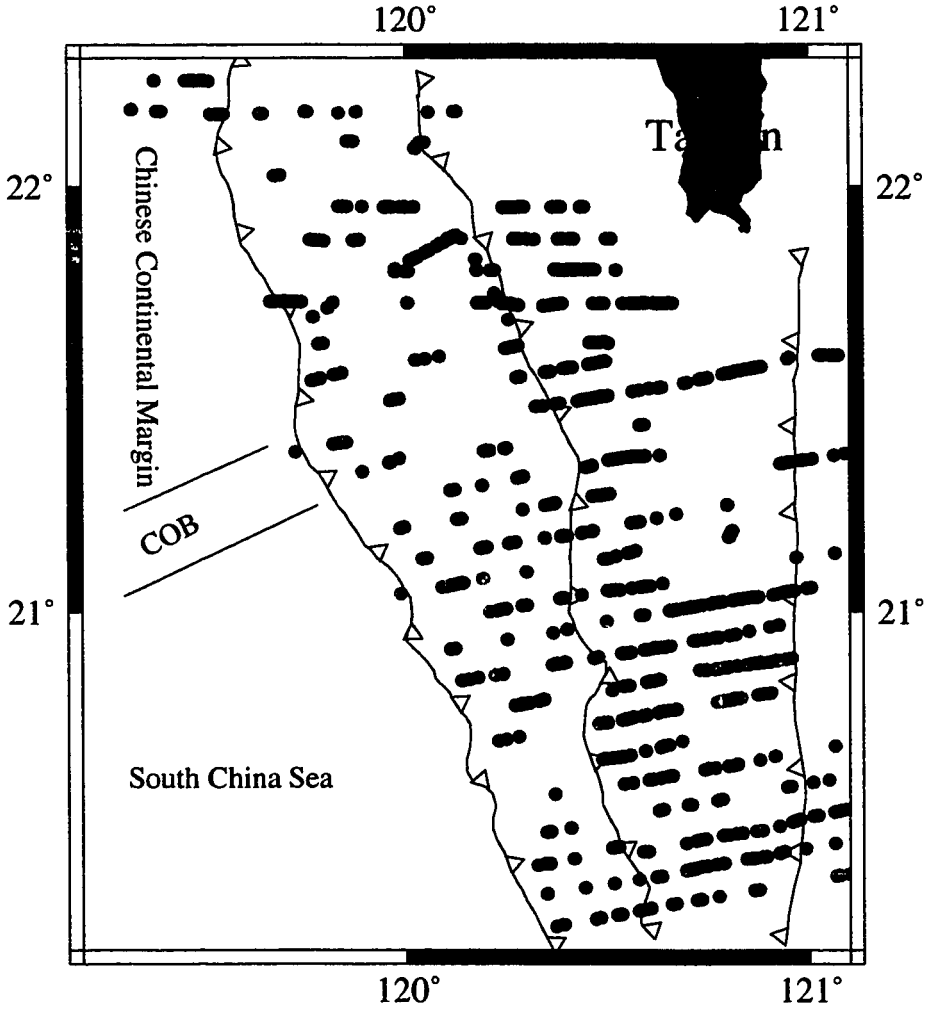

Figure 8c: Distribution of the possible type (Q3) BSRs.

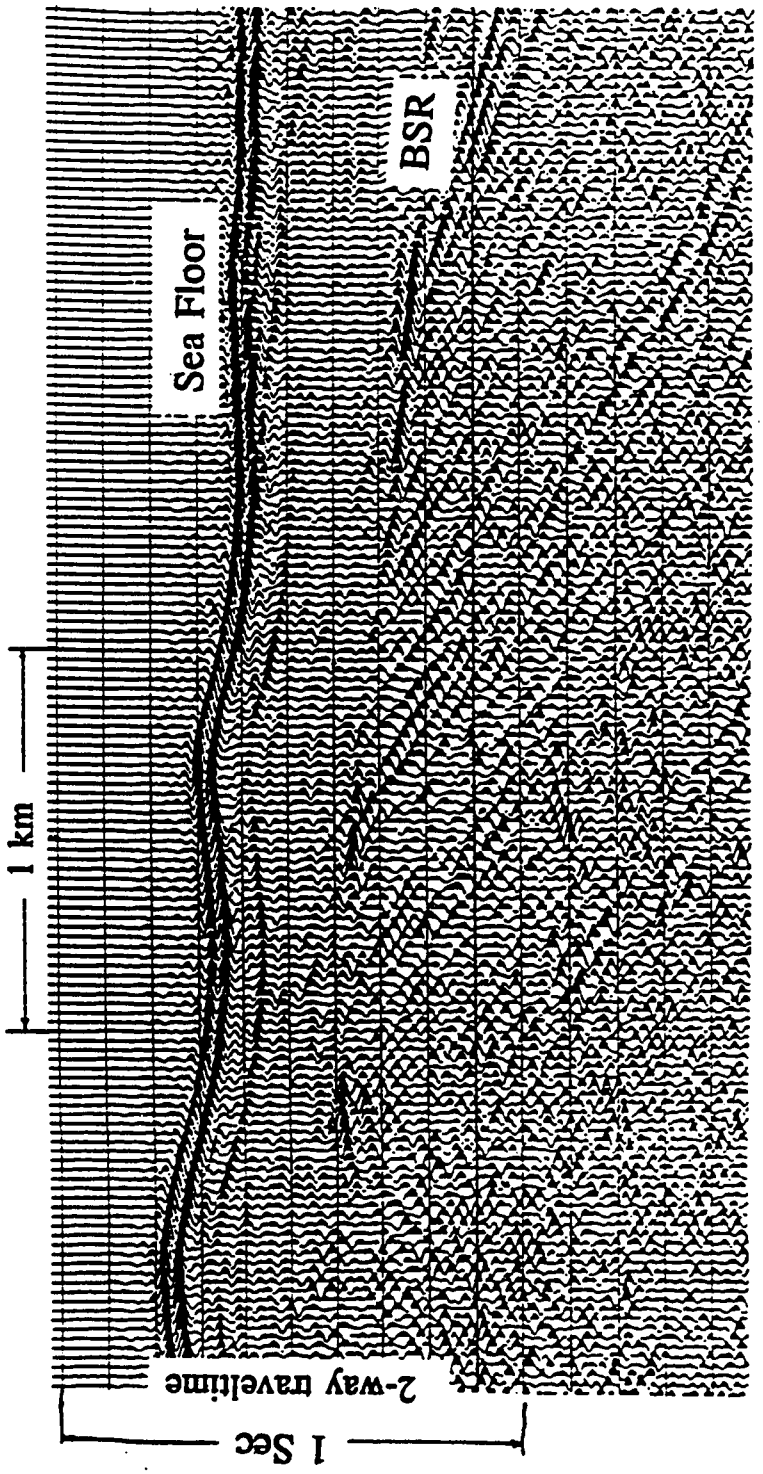

Figure 9. BSR sub-bottom depth increases as water depth increases. Note reverse polarity of BSR. See site I on Figure 7 for location.

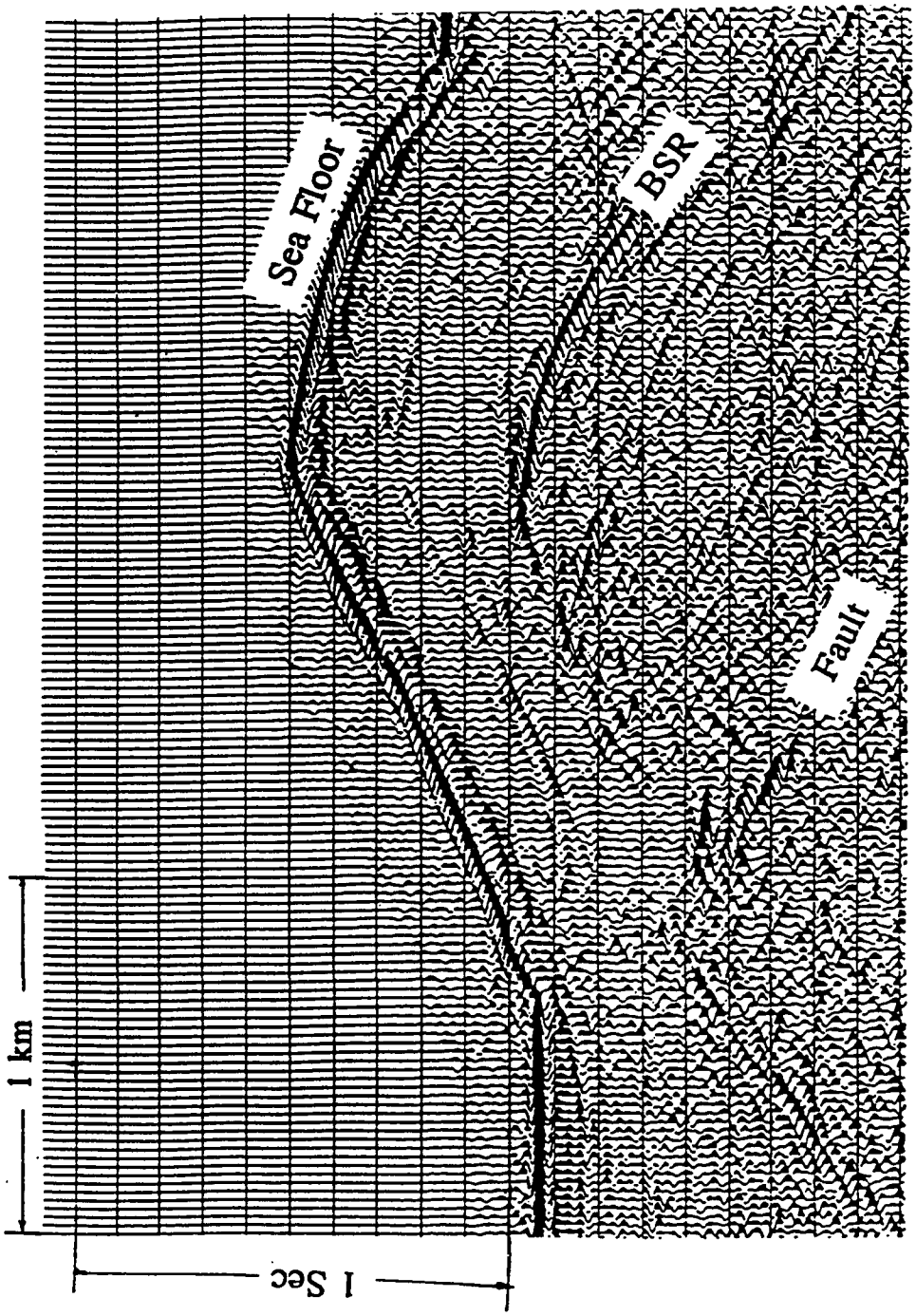

Figure 10. BSR shallows toward a fault zone despite increase in water depth. See site II on Figure 7 for location.

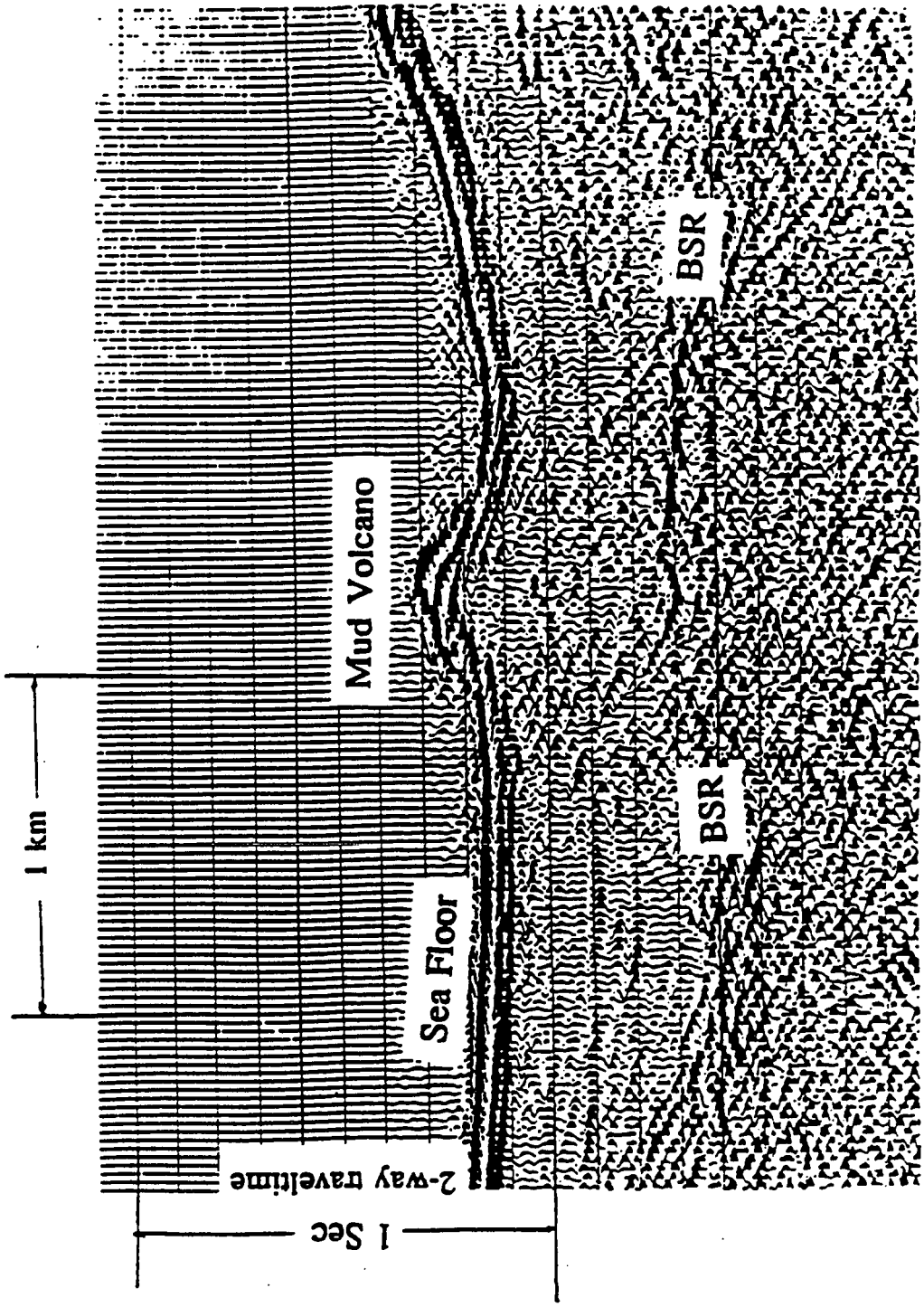

Figure 11. BSR shallows beneath a mud volcano. See site III on Figure 7 for location.

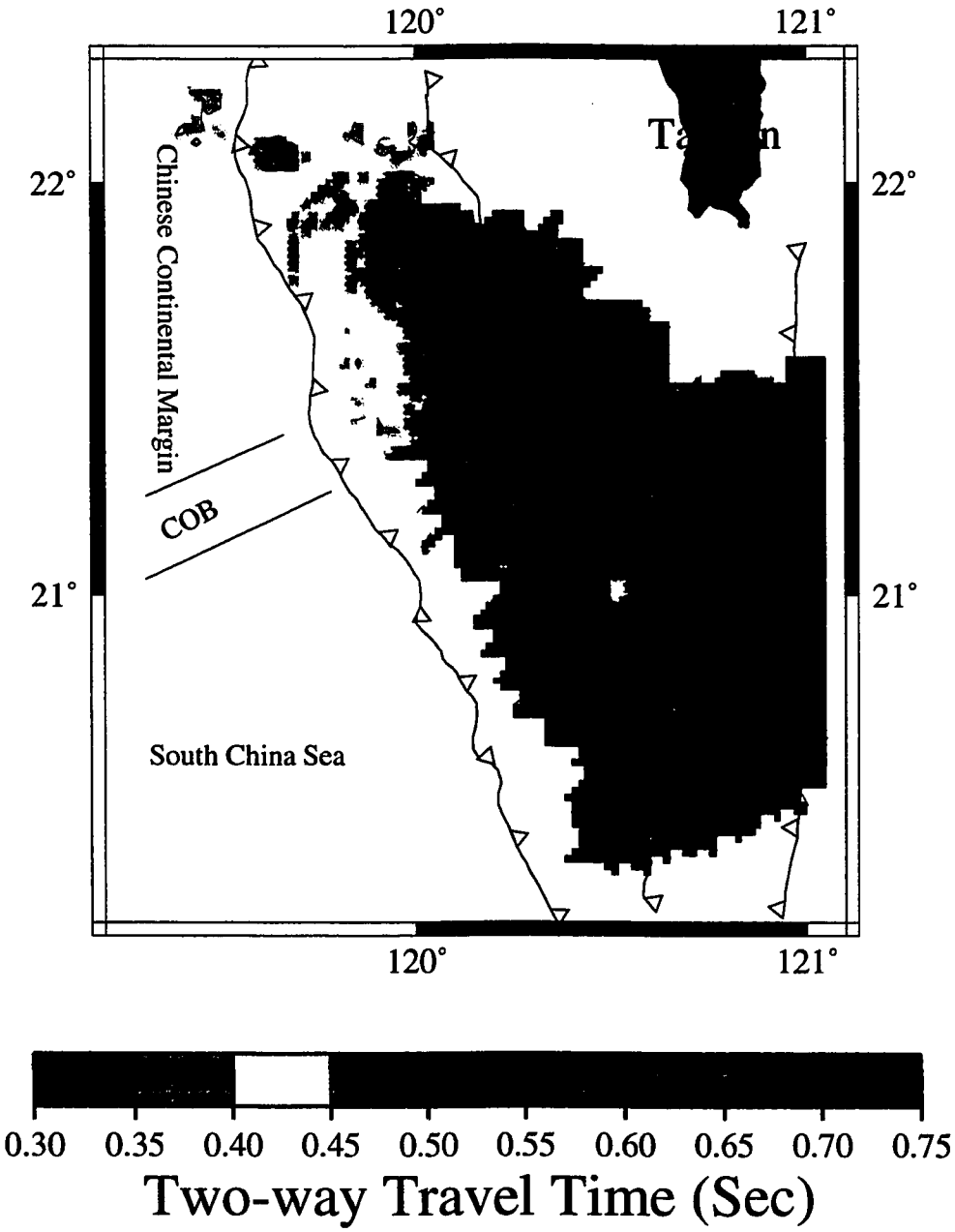

Figure 12: Contour map of BSR sub-bottom depth.

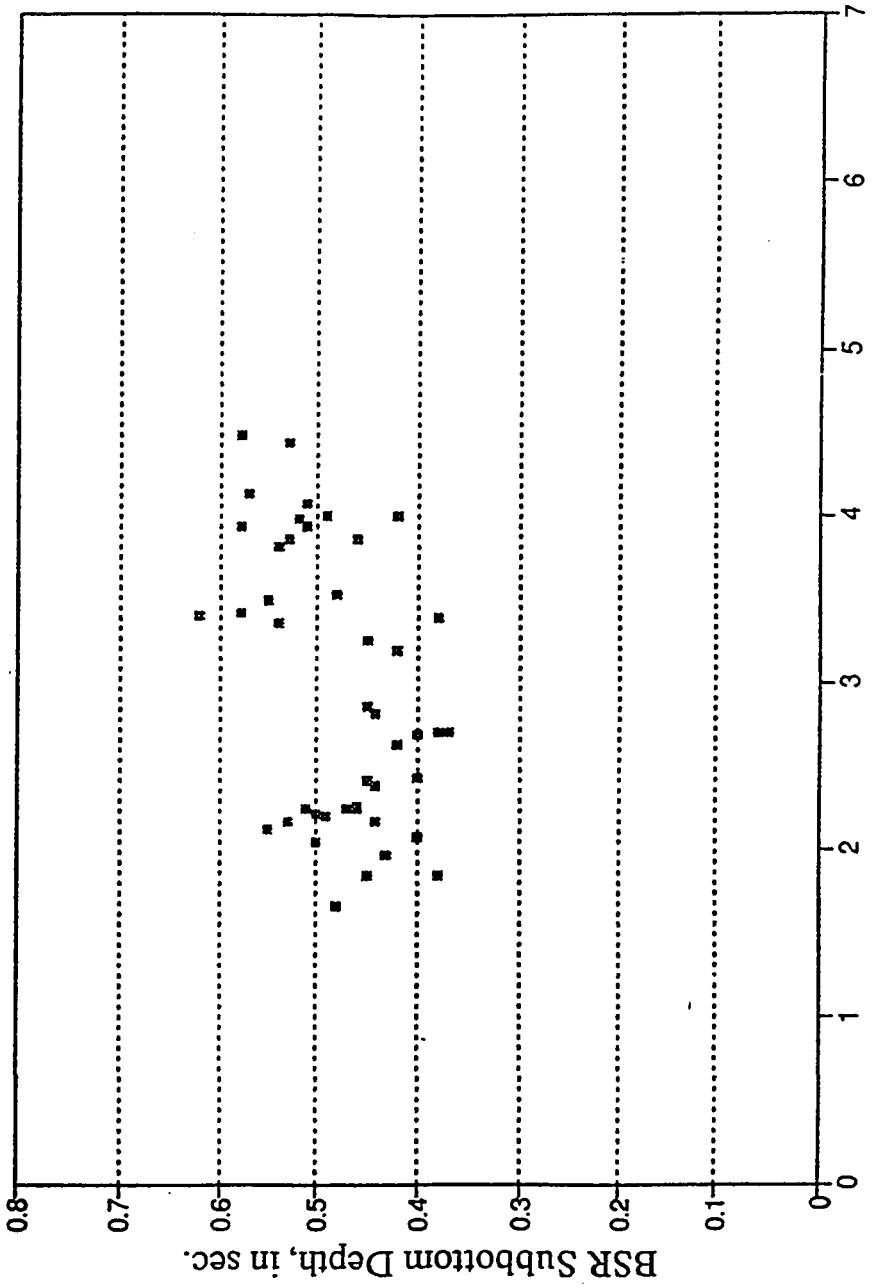

Figure 13a. Clear type (Q1) BSR Sub-Bottom Depth vs. Water Depth in seconds (two-way traveltime).

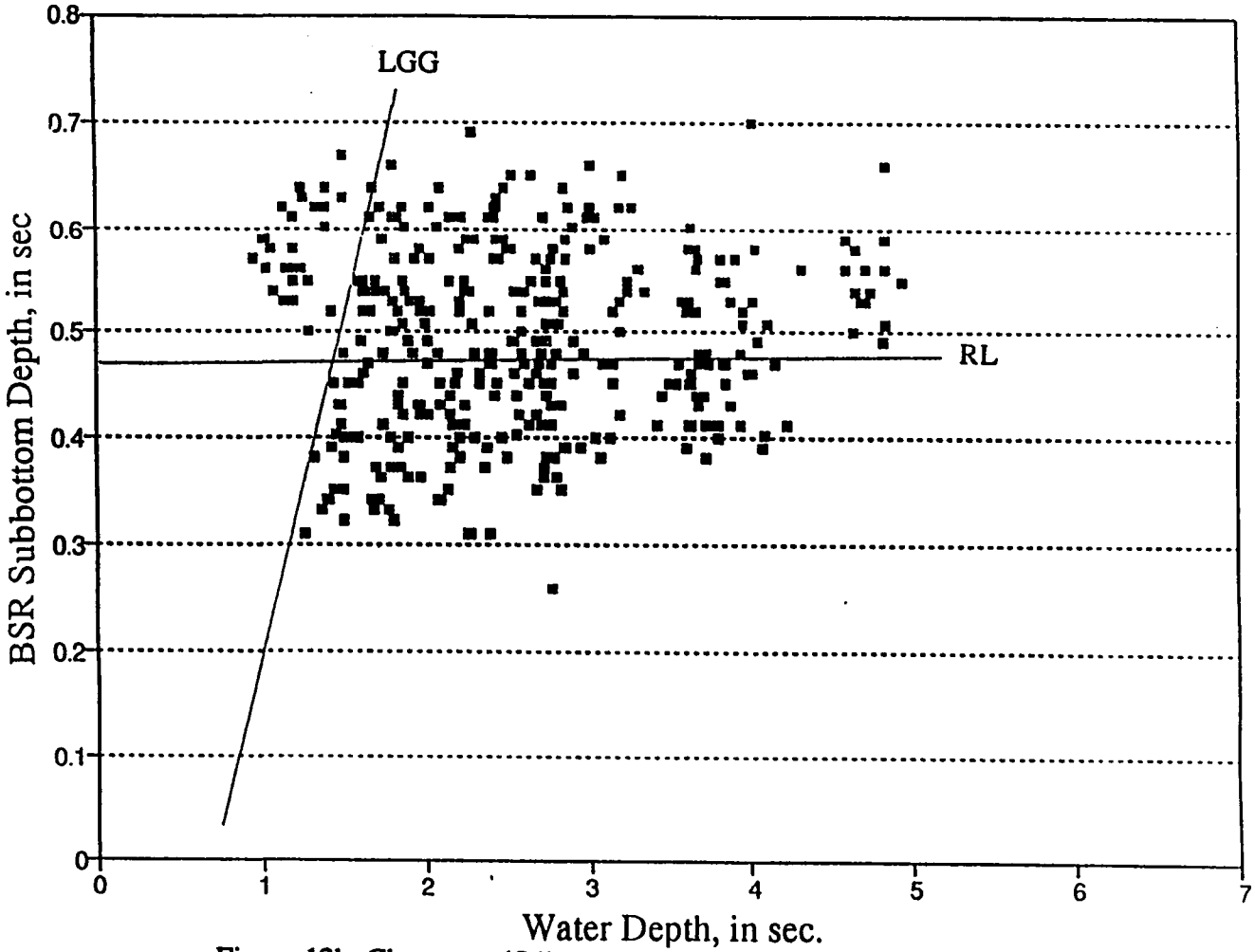

Figure 13b. Clear type (Q1) and Probable type (Q2) BSR Sub-Bottom Depth vs. Water Depth in seconds (two-way traveltime). RL: regression line. LGG: possible regional lowest geothermal gradient, if some abnormal data on the left of the LGG line are ignored.

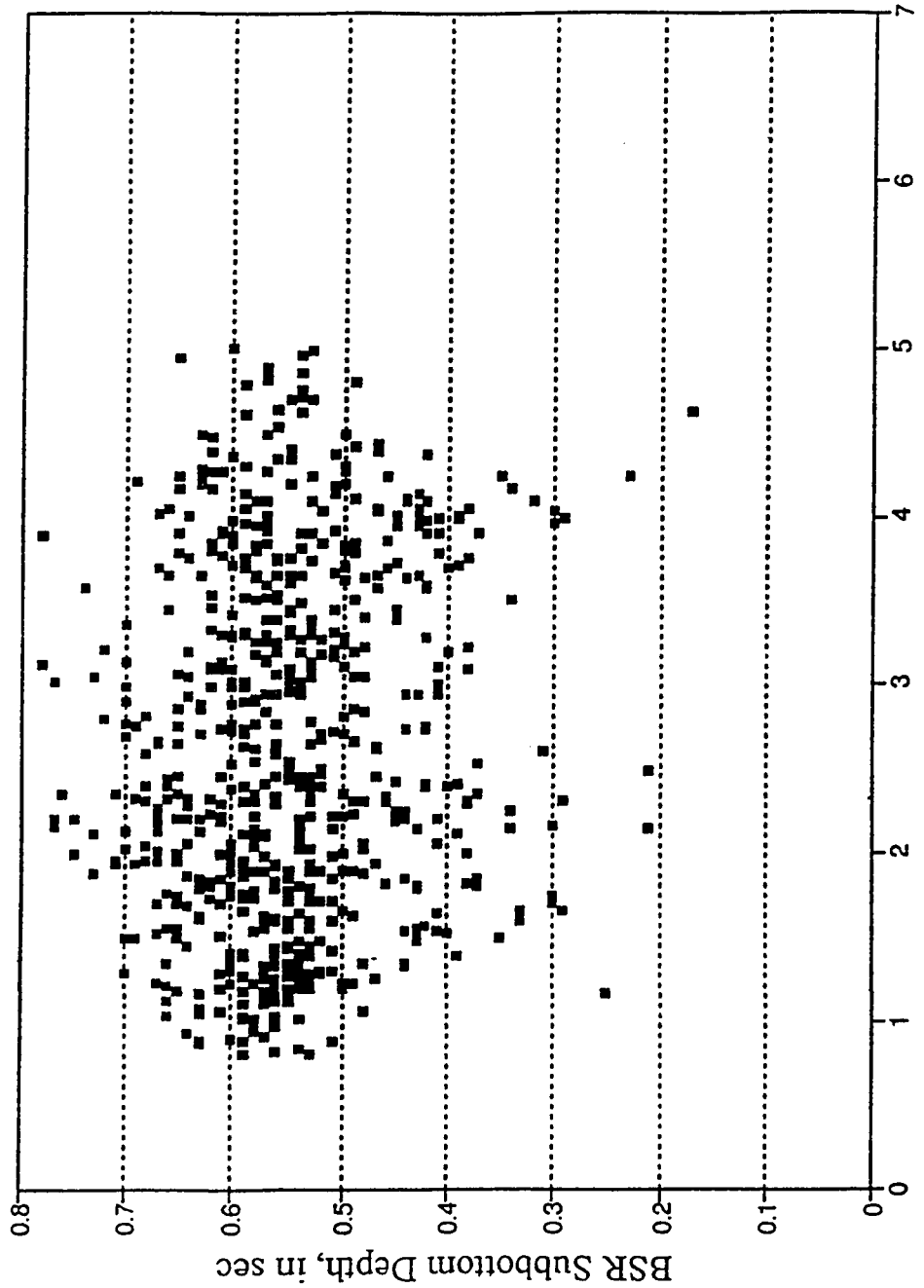

Figure 13c. Possible type (Q3) BSR Sub-Bottom Depth vs. Water Depth in seconds (two-way traveltime).

reflectors that fit all the seismic characteristics of the BSR are assigned highest quality (Q1); Q2 was assigned to the probable BSRs; Q3 was assigned to the possible BSRs. For the highest quality (Q1) BSR depths, BSR sub-bottom depth generally increases with increasing water depth (Fig. 13a). On the other hand, points are scattered on the intermediate quality (Q2) BSR plot, which includes Q1 points (Fig. 13b). In order to obtain a general trend of water depth vs. BSR sub-bottom depth in this region, a regression technique was employed to Q2 data to define the following equation:

$$D_{BSR}=0.470+0.008\times D_{WATER}$$

D_{BSR}: BSR sub-bottom depth in seconds (two-way traveltime)

D_{WATER}: Water depth in seconds (two-way traveltime)

The observed BSR sub-bottom depth was compared to the BSR sub-bottom depth predicted from the regression equation. Maps of distribution of BSRs associated with either shallower- or deeper-than-expected sub-bottom depth are displayed in Figures 14a and 14b, respectively. BSRs with shallower-than-expected sub-bottom depth are mostly located in the collision zone and the lower slope domain near the collision zone, whereas BSRs with deeper than predicted sub-bottom depths are located in the upper slope domain, in the southern part of the lower slope domain, and near the lower-upper slope domain boundary in the collision zone.

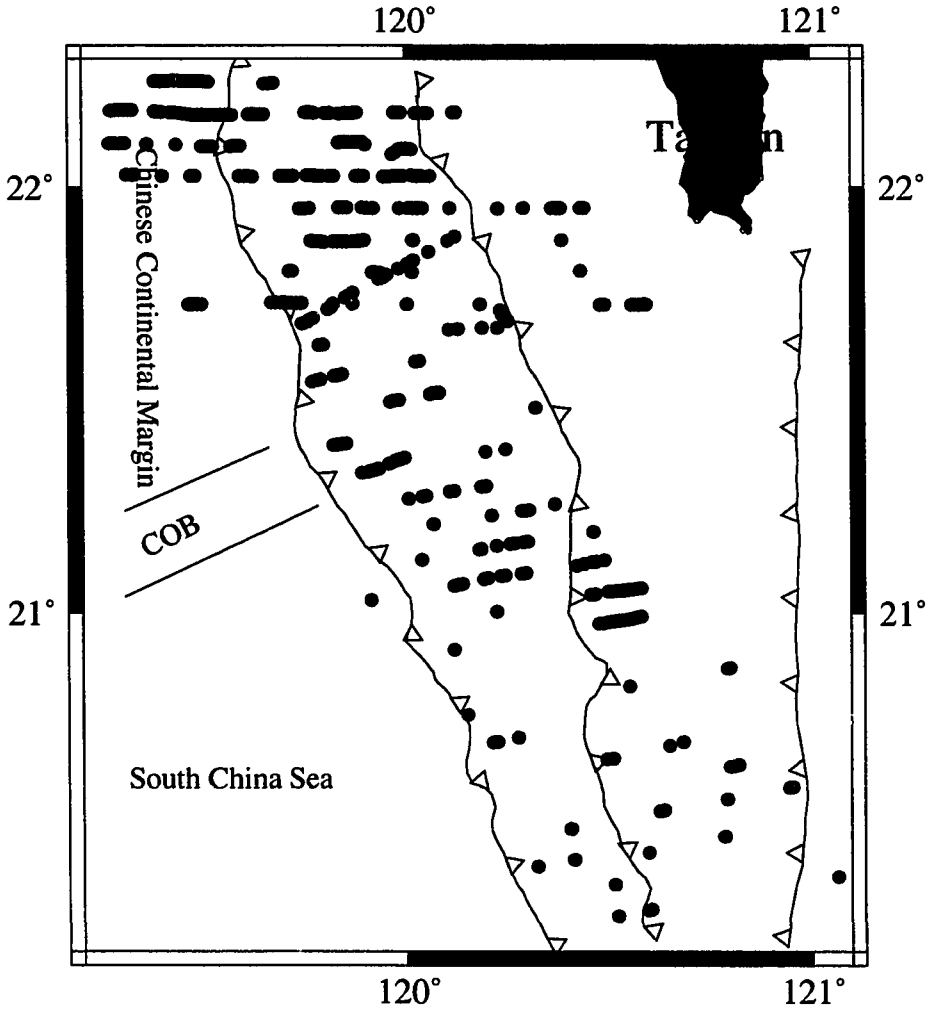

Figure 14a. Distribution of all BSRs with shallow-than-expected sub-bottom depth.

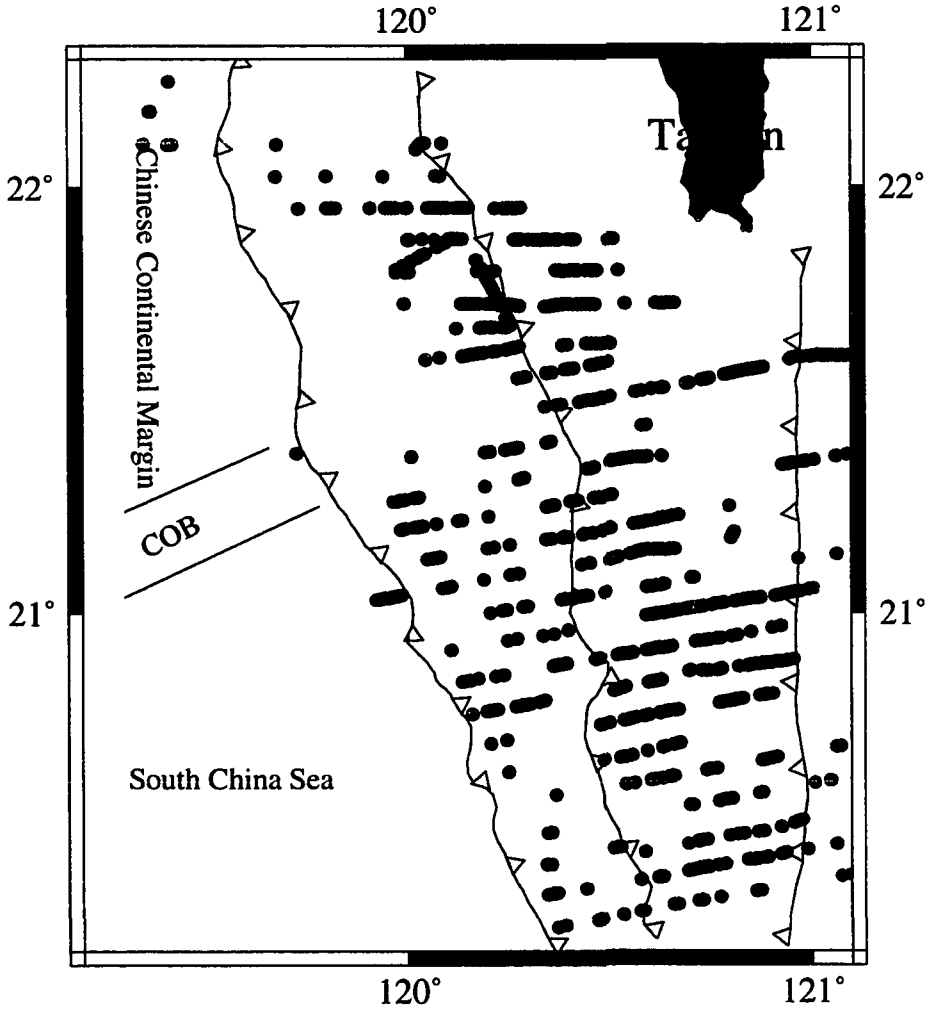

Figure 14b. Distribution of all BSRs with deeper-than-expected sub-bottom depth.

DISCUSSION

Sediment Types and the Distribution of BSRs

The concentration of BSRs is highest in the northwest region of the study area (Fig. 8a, 8b). The sediments in this region are composed of offscraped terrigenous detritus derived from the Chinese continental margin and uplifted Taiwan orogen. The fine-grained fraction of rapidly deposited terrigenous sediments commonly has relatively high amounts of organic carbon, compared to pelagic sediment of the ocean basin (Selley, 1983). The organic carbon contained in offshore Taiwan strata may be the source of methane in the region, which has contributed to the formation of the hydrate layer. Many BSRs may be related to possible updip gas migration underneath the methane hydrate layer, implied by their location in the crests of anticlines.

Many studies have suggested that free gas is trapped beneath the BSRs in other regions (Miller and others, 1991; Singh and others, 1993; Bangs and others, 1993; ODP Leg 146 Scientific Party, 1993; Singh and others, 1993; MacKay and others, 1994). Direct hydrocarbon indicators (Fig. 15), in the form of high amplitude "flat spots" are found underneath the BSRs in several regions of the Taiwan accretionary prism (Chi and others, 1993), implying that the reduced permeability in hydrate-filled pore space may trap gas underneath the methane hydrate layer.

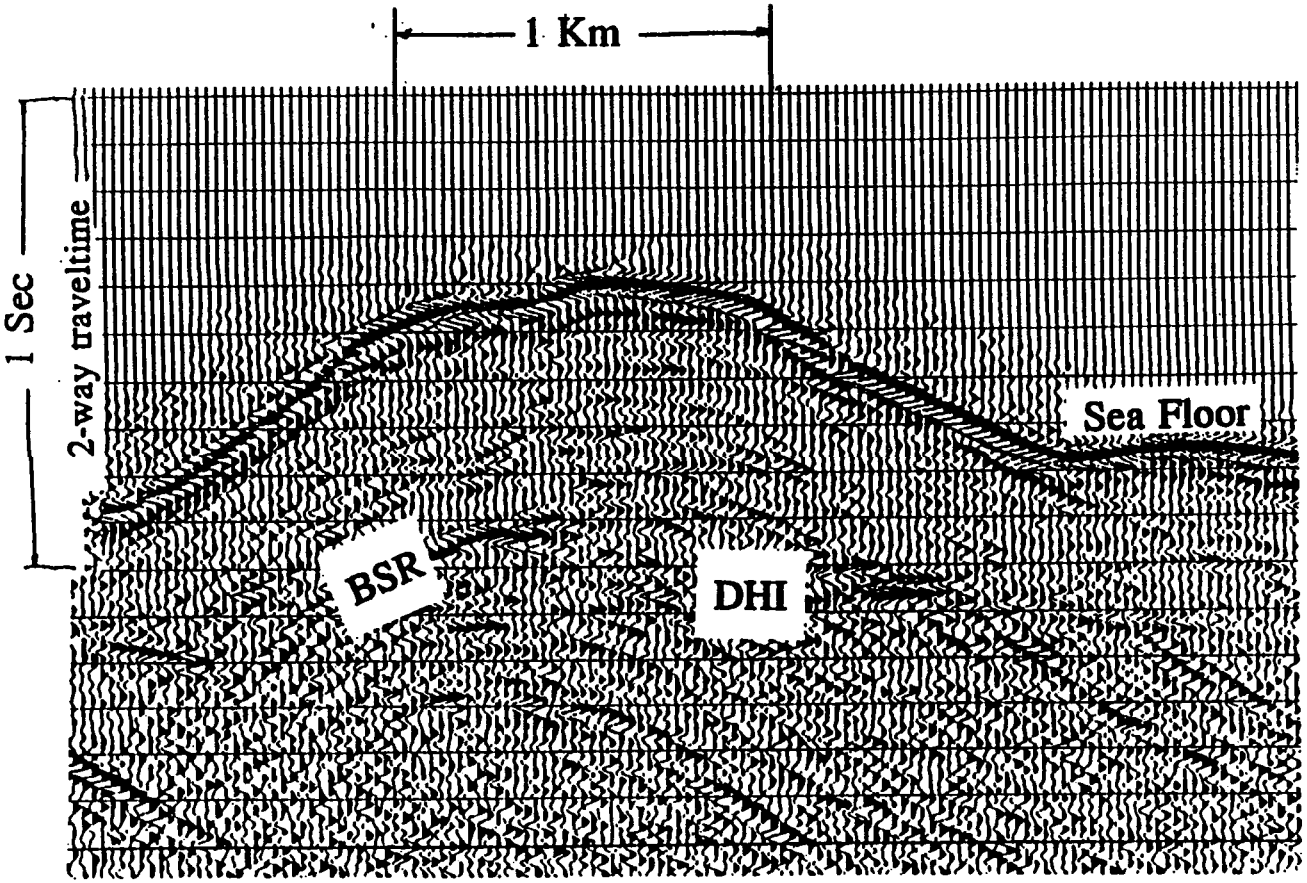

Figure 15. Direct hydrocarbon indicator (DHI) underneath the BSR. See site IV on Figure 7 for location.

Implications of BSR Sub-bottom Depth

As shown on figure 12, BSR sub-bottom depths differ from place to place. Uncertainties in measuring the two-way traveltime of the seafloor and the BSR are less than 0.05 second and therefore significantly less than the range of BSR measurements. Sub-bottom depths of BSRs in two-way traveltime can be influenced by a number of factors, including: (1) lateral variations in sediment velocity above the BSR, (2) variable chemical composition of gas hydrate and changes in methane supply, and (3) spatial and temporal changes in P-T conditions.

Currently, few data have been acquired on offshore sediment velocities around southern Taiwan; likewise the chemical composition of gas hydrate in the region is unknown. However, studies elsewhere have found little velocity variation (<8%) between surface sediments that contain gas hydrate and those that do not, such as in the accretionary prism off Oregon and Washington (Hyndman and others, 1992; Mackay and others, 1994). BSR depth variations associated with the relative proportions of methane, ethane, and propane contained in gas hydrate also appear to be minor (Kvenvolden, personal commun., 1994). Consequently, variations in BSR sub-bottom depths, particularly along the surface of modern accretionary prisms, are commonly attributed to changing P-T conditions beneath the seafloor. Bodnar and others (1994) have shown that gas hydrate stability responds rapidly to changes in P-T conditions, so that BSR depths reflect the modern P-T regime.

The two most prominent effects on P-T conditions in near-surface sediments are

water depth and geothermal gradient. The BSR sub-bottom depth around southern Taiwan generally increases with increasing water depth, implying suppression of the hydrate stability field due to increasing hydrostatic pressure and decreasing bottom water (seafloor) temperature.

The variation in the general trend of BSR depths in the Q1 plot (Fig. 13a) is mainly due to its occurrence in regions of folded strata. Figure 16 shows that the curvature of the BSR is slightly less than that of the sea floor topography. A similar pattern is shown in seismic profiles from the western North Atlantic (Tucholke and others, 1977). This observation may relate to the fact that the shortest distances between seafloor and isotherms are not vertical; as a result, the direction of heat flow near the crest of an anticline is deflected limbward, causing more heat transfer near the limbs compared with less heat transfer near the crests of anticlines. Therefore, BSR sub-bottom depth increases toward the crests of anticlines and the summits of mud volcanoes in several regions, despite the decreasing water depth. A second factor contributing to the scattering in the plot of BSR depths vs. water depths might be variations in geothermal gradients.

Scattering of data points in the Q2 plot (Fig. 13b) strongly suggests spatial variations in geothermal gradient. The Q2 plot is similar to that compiled in another study of the Blake Outer Ridge (figure 7 of Tucholke and others, 1977). The line drawn in figure 13b may represent the BSRs with lowest regional geothermal gradient.

BSRs are shallower than expected at fault zones and beneath mud volcanoes within the lower slope domain and the collision zone, and show high relief over short distances.

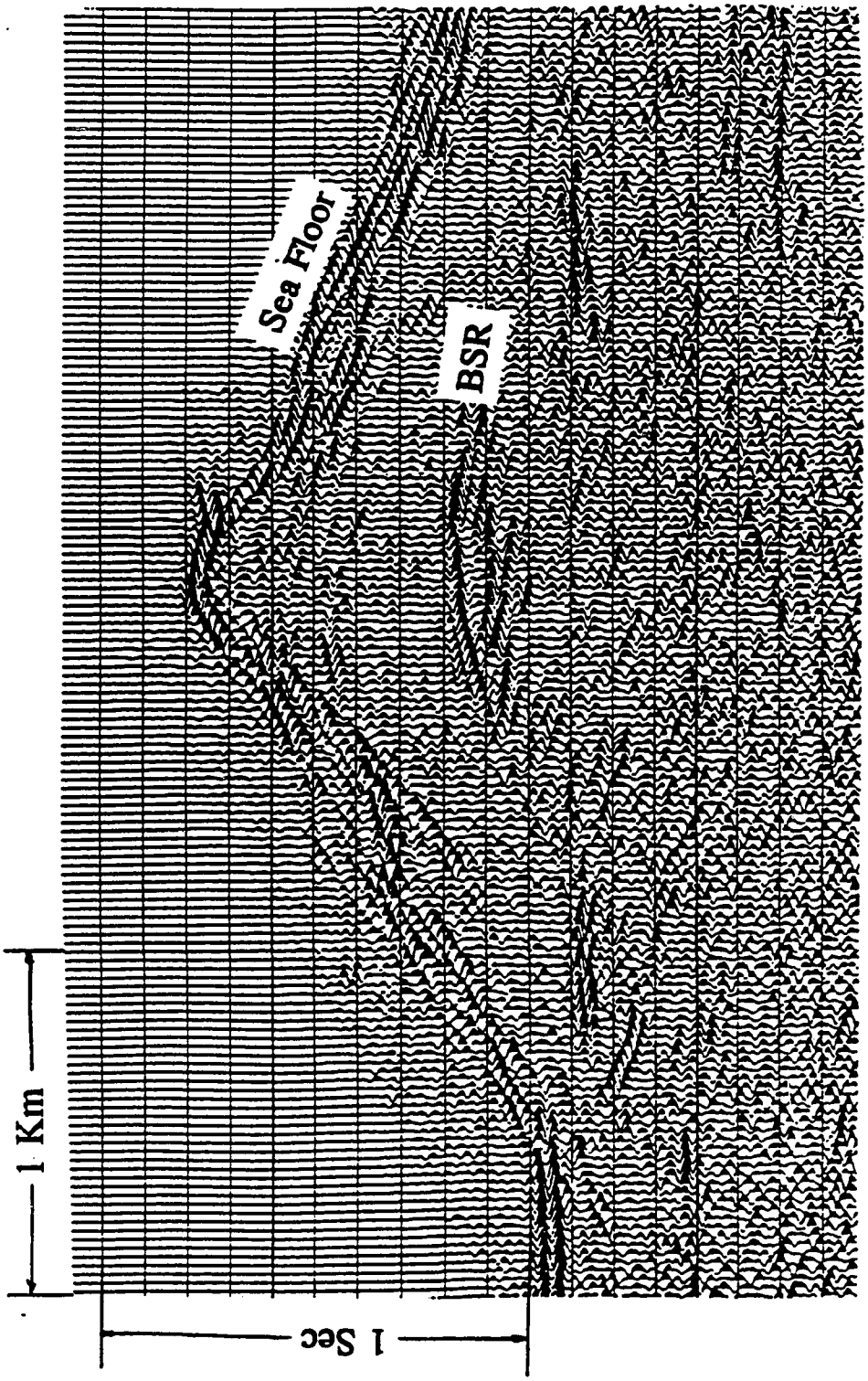

Figure 16. Variations of BSR sub-bottom depth, which could be contributed by the tight curvature of seafloor topography. See site V on Figure 7 for location.

The measured relief on the BSRs is too large to be related solely to velocity anomalies. Moreover, there is no evidence of a velocity pull-up of the stratigraphy below BSRs, implying that the high relief of the BSR is associated with changes in P-T conditions.

BSR Depth as Evidence of Fluid Migration

Heat-flow variation probably is the main factor causing the shallowing of the BSR at fault zones and beneath mud volcanoes, although pressure variation could also contribute to part of the variations in BSR sub-bottom depth. Rowe and Gettrust (1993) studied offsets of the BSR of up to 20m across faults in the Blake Outer Ridge and interpreted these offsets as a result of 0.2 MPa pressure changes across the fault zone. However, the magnitude of variations in BSR sub-bottom depths near fault zones around southern Taiwan requires at least 10 MPa pressure difference (or 8°C temperature difference), if geothermal gradients are consistent in the region; there is no evidence of such great pressure difference across fault zones. Indeed, the seismic profiles show no sharp "offset" of BSRs across these fault zones in this region. Therefore, lateral temperature variations on the order of 8°C, as inferred from the BSR relief and the hydrate phase equilibria, are the most likely factor controlling the shallowing of BSRs at fault zones. Such temperature variations may indicate active fluid migration from depth along fault zones, which may also account for the fault plane reflections, implying high fluid pressures along the fault zones (Reed and others, 1991).

A Model of Geothermal Gradient in Offshore Taiwan Accretionary Prism

Assuming the BSR sub-bottom depths accurately reflect P-T conditions beneath the seafloor around southern Taiwan, a thermal model is derived that can be tested with future ocean drilling in the region. In order to calculate the geothermal gradient from BSRs, one needs (1) the BSR sub-bottom depth in meters, (2) temperature at the BSR, and (3) temperature at seafloor. Unfortunately, there is no drilling dataset available to get all of this information. However, the following calculation is based on available data from accretionary prisms elsewhere in the world.

Two-way traveltime of BSR sub-bottom depth was converted into BSR sub-bottom depth in meters by using velocity-depth relations published by Hamilton (1980):

$$H_{BSR} = V_{AVG} \times t$$

$$= [1511 + (1041 \times t) - (372 \times t^2)] \times t$$

H_{BSR}: BSR sub-bottom depth, in m

V_{AVG}: Average velocity of sediments above BSR, in m/sec

t: One-way traveltime of BSR sub-bottom depth, in sec

This empirical equation does not consider velocity increases due to pore-filled hydrate. However, regions of hydrate in the Cascadia accretionary prism exhibit a velocity anomaly of less than 100 m/s (c.f. MacKay and others, 1994). Velocity variations of this

magnitude around southern Taiwan would result in a difference of less than 50 m in the sub-bottom depth conversion.

The two-way traveltime to the seafloor was divided by two and converted into water depth in meters (H_{WATER}) by assuming 1500 m/sec as the seismic velocity of water. An empirical equation was derived to reproduce the methane hydrate phase boundary data published by Hyndman and Davis (1992):

$$T_{BSR}=2.03\times[\log(H_{WATER}+H_{BSR})-2]\times 9.75-4$$

T_{BSR}: Temperature at BSRs, in °C

Another equation was derived to represent the sea floor temperature by using the data from Kvenvolden and McMenamin (1980):

T_{SF} = 4 for $H_{WATER} < 1500m$

= 4-(water depth-1500)/600 for $1500m < H_{WATER} < 3300m$

= 1 for $H_{WATER} > 3300m$

T_{SF}: Temperature at sae floor, in °C

These two quantities were combined to determine geothermal gradient according to following equation:

Geothermal gradient = $(T_{BSR} - T_{SF}) / H_{BSR}$

Geothermal data were next compiled into a geothermal gradient contour map (Fig. 17). The regional geothermal gradient ranges from 17 to 160°C/km, with most values between 20 and 40 °C/km. An uncertainty of 30% in this estimate (c.f. Ashi and Taira, 1993) would cause only 6-12 °C/km difference. Uncertainties in the estimates here should be systematic. Consequently I direct this analysis towards relative variations in geothermal gradient not the absolute value.

Dewatering near the Toe of the Accretionary Prism

The contour map in figure 17 shows an increase in geothermal gradient toward the toe of the accretionary prism, as has been observed in the Nankai and Oregon accretionary prisms (Yamano and others, 1992; Zwart and Moore, 1993). This increase could be due to (1) higher fluid flux due to sediment dewatering near the frontal thrust, and (2) a decrease in the "thermal blanketing effect" due to thinning of sediment thickness towards the toe of the accretionary prism.

Several studies have shown that sediment dewatering and presumably fluid flow are most extensive along the toe of accretionary prisms (Bray and Karig, 1985). Fluids are also released by dehydration reactions within sediments. These fluids are forced to migrate upwards, advecting heat. Large geothermal gradient anomalies are confined to the regions of mud volcanoes and fault zones. Other evidence of overpressures and fluid

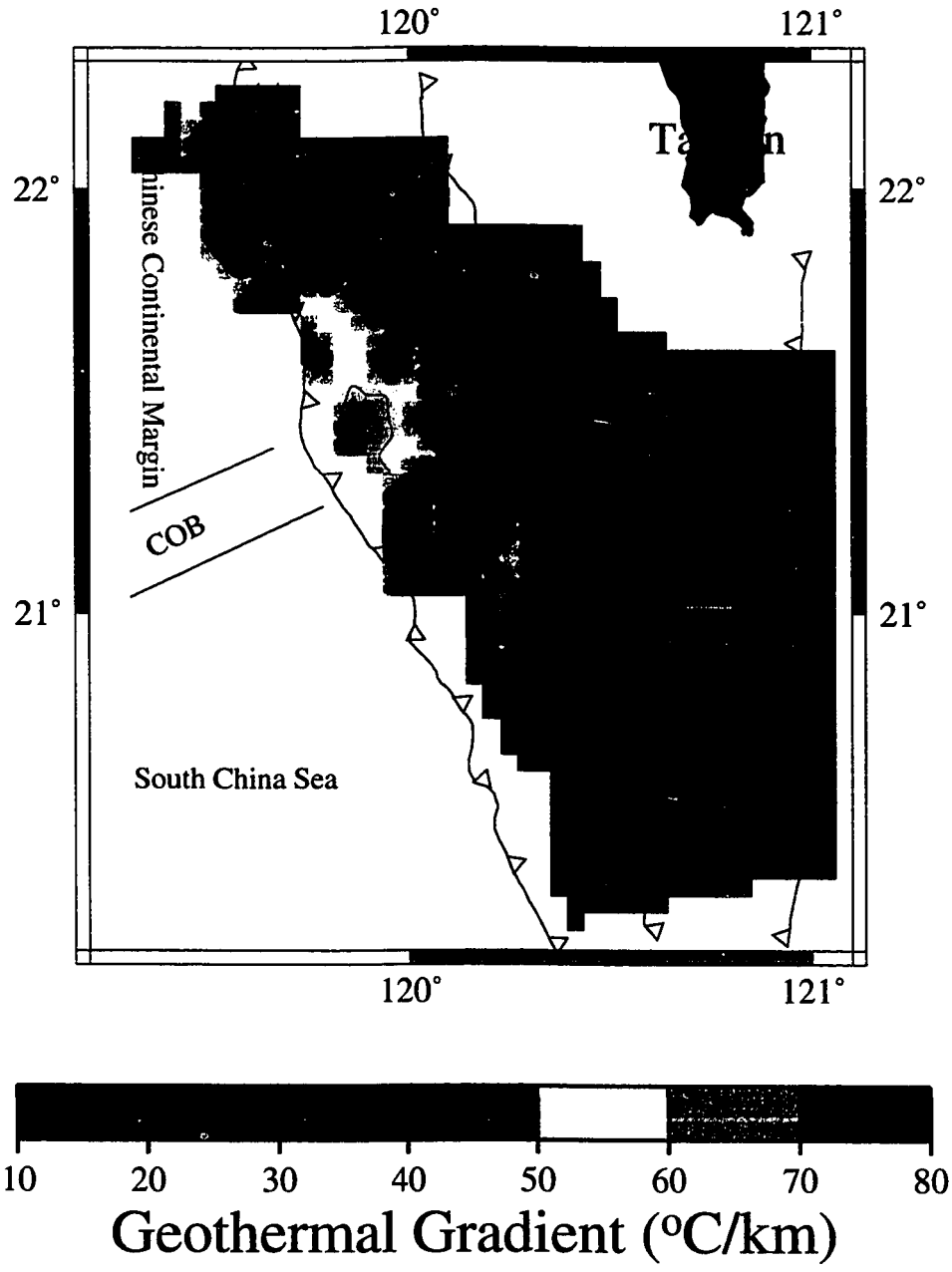

Figure 17: Contour map of estimated geothermal gradient

migration within the lower slope domain, especially in the collision zone, includes bright spots beneath BSRs and fault zones, the presence of mud volcanos, and the small taper angle of the prism (Reed, unpublished data).

A second factor causing the variations in geothermal gradient is the blanketing effect of sediment above the oceanic crust. The thicker section of upper slope sediments acts as an insulator, thereby reducing the geothermal gradient near the seafloor, whereas thinner sediment accumulations along the lower slope have a lower insulating capacity, producing a higher geothermal gradient.

Contours of geothermal gradient are parallel to the structural trends (c.f. Fig. 17, 18). If geothermal gradient variations are mainly controlled by tectonically-induced sediment dewatering and blanketing, this parallelism suggests that the dewatering and blanketing effects are structurally controlled by the growth of the accretionary prism. Also, from south to the north, the calculated geothermal gradients (Fig. 14a, 17) increase where the structural lineations change orientation from north-south in the region of subduction to NW-SE in the collision zone, and where the width of accretionary prism increases dramatically, due to the accretion of Chinese continental margin strata and sediments of the Taiwan orogen (Fig. 18).

Low Geothermal Gradient near the Boundary of Upper and Lower Slope Domains

Geothermal gradients are particularly low near the boundary of upper and lower slope domains (Fig. 14b). A similar thermal pattern near the frontal thrust on land in

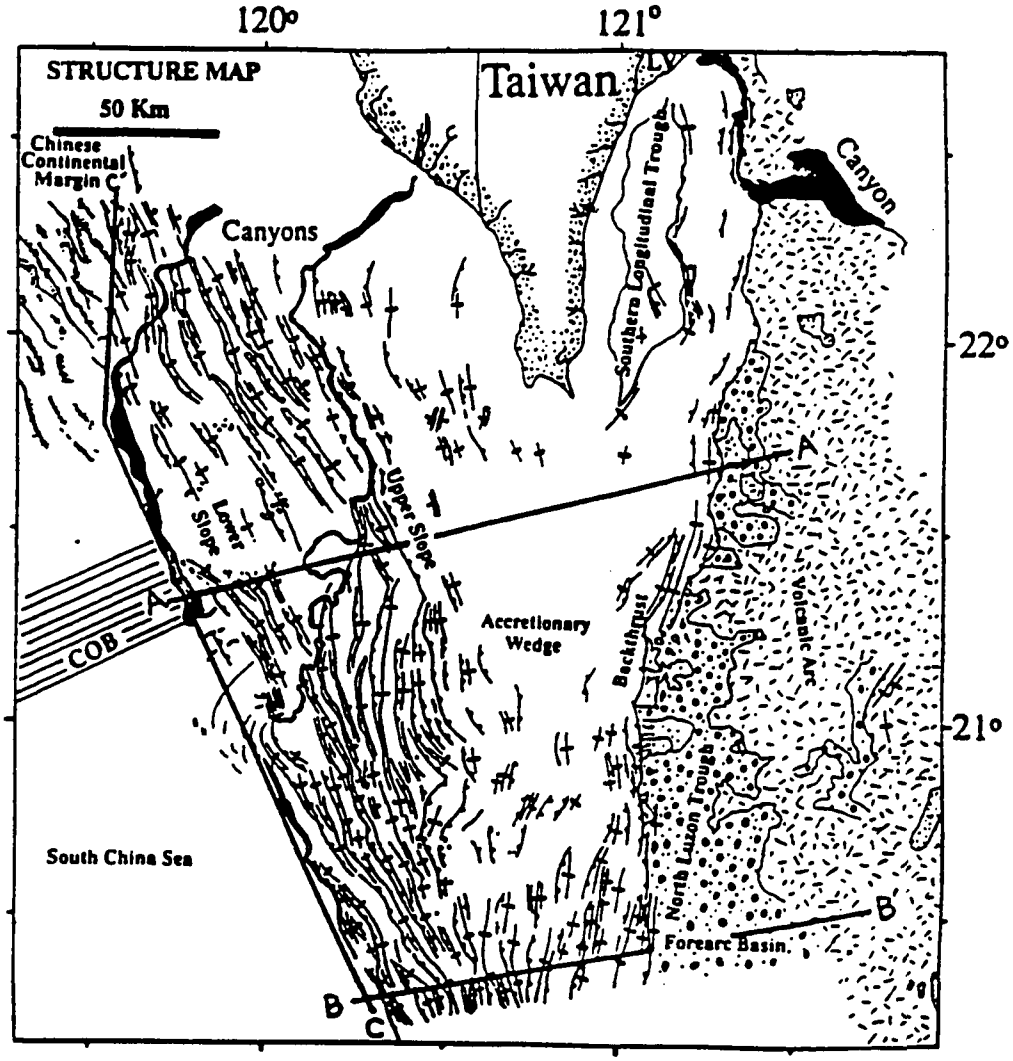

Figure 18. Structural map of study area (after Reed and others, 1992).

northern Taiwan was interpreted by Hwang and Wang (1993) as the result of stacking of cold sediment layers by thrusting. If this is the case in the study area, it implies that intensely deformed and less porous upper slope sediments have been thrust on top of the lower slope strata, thereby thickening the sediment layer over the subducting crust. The low geothermal gradient also could be a result of decreased fluid migration, because most porosity reduction usually occurs within a few tens of kilometers landward of the deformation front in accretionary prisms (Bray and Karig, 1985, Breen and Orange, 1992).

Possible Heat Flow Value Range

Assuming a thermal conductivity of 0.882 W/mK for terrigenous sediments (Stein and Abbott, 1991), heat flow values were estimated at 15-141 mW/m^2. However, most of the study area has heat flow values ranging between 20-40 mW/m^2. The age of the subducting oceanic crust implies a heat flow of 84 mW/m^2, according to the age-heat flow equation of Parsons and Scalter (1977). The lower observed heat flow values estimated in the offshore Taiwan accretionary prism may be due to the blanketing effect of cold sediments on top of the subducting crust, as is observed in many accretionary prisms (Yamano and Others, 1992; Zwart and Moore, 1993).

CONCLUSIONS

The BSR around southern Taiwan represents the base of a methane hydrate layer. The BSR has a reversed polarity and increases in sub-bottom depth with increasing water depth. The BSR is widespread in areas of the accretionary prism composed of offscraped sediments of the Chinese continental margin and the Taiwan orogen, which may reflect high amounts of organic carbon in rapidly deposited terrigenous sediments. These organic materials may produce either thermogenic or biogenic methane, and other gases, which migrate into anticlines and form gas hydrates. Bright spots located underneath the BSR suggest fluid migration and possible gas entrapment below the hydrate layer.

Geothermal gradient was estimated by using BSR sub-bottom depth, methane hydrate phase equilibria, and seafloor temperature data. Regional geothermal gradient ranges from 17 to 160 ^{o}C/km with most values between 20-40 ^{o}C/km . The variations of geothermal gradient may be due to sediment dewatering during offscraping and the blanketing effect of sediment on top of the subducting oceanic crust. Local deviations in geothermal gradient were found at fault zones and underneath mud volcanoes, implying focused fluid flow. Geothermal gradient increases towards the toe of the accretionary prism, implying less blanketing effect and possible diffuse flow in that region.

REFERENCES CITED

Ashi, J., and Taira, A.,1993, Thermal structure of the Nankai accretionary prism as inferred from the distribution of gas hydrate BSRs, in Underwood, M.B., ed., Thermal evolution of the Tertiary Shimanto Belt, southwest Japan: An example of ridge-trench interaction: Geological Society of America Special Paper 273, p.137-149.

Bangs, N.L.B., Sawyer, D.S., and Golovchenko, X., 1993, Free gas at the base of the gas hydrate zone in the vicinity of the Chile triple junction: Geology, v.21, p.905-908.

Bray, C.J., and Karig, D.E., 1985, Porosity of sediments in accretionary prisms and some implications for dewatering processes: Journal of Geophysical Research, v.90, p.768-778.

Breen, N.A., and Orange, D.L., 1992, The effects of fluid escape on accretionary wedges 1. variable porosity and wedge convexity: Journal of Geophysical Research, v.97, p.9265-9275.

Chi, W.-C., Reed, D.L., Lundberg, N., and Liu, C.-S., 1993, Distribution of the Bottom-Simulating Reflector in the offshore Taiwan collision zone: implications for fluid migration (abs.): EOS, Transactions, American Geophysical Union, Supplement, v.74, p.583.

Froelich, P.N., Kvenvolden, K.A., Torres, M., and Leg 141 Shipboard Scientific Party, 1993, Evidence for gas hydrate in the accretionary prism near the Chile triple junction -- ODP Leg 141: EOS, Transactions, American Geophysical Union, Supplement, v.74, p.369.

Gamo, T., Sakai, H., Ishibashi, J.-i, Shitashima, K., and Bouleque, J., 1992, Methane,ethane and total inorganic carbon in fluid samples taken during the 1989 Kaiko-Nankai project: Earth and Planetary Science Letters, v.109, p.383-390.

Guinasso, N.L. Jr., MacDonald, I.R., Brooks, J.M., Sassen, R., and Scott, K.M., 1994, Seafloor gas-hydrates: a video documenting oceanographic influences on their formation and dissociation: 1994 ocean sciences meeting, EOS, Transactions, American Geophysical Union, supplement, v.75, p.175.

Hamilton, E.L., 1980, Geoacoustic modeling of the sea floor: Journal of Acoustical Society of America, v.68, p.1313-1339.

Hwang, W.-T., and Wang, C.-y., 1993, Sequential thrusting model for mountain building: constraints from geology and heat flow of Taiwan: Journal of Geophysical Research, v.98, p.9963-9973.

Ho, C.S., 1986, A synthesis of the geologic evolution of Taiwan: Tectonophysics, v.125, p.1-16.

Hyndman, R.D., and Davis, E.E., 1992, A mechanism for the formation of methane hydrate and seafloor Bottom-Simulating-Reflectors by vertical fluid expulsion: Journal of Geophysical Research, v.97, p.910-924.

_____, and Foucher, J.P., Yamano, M., Fisher, A., and Scientific Team of Ocean Drilling Program Leg 131, 1992, Deep sea bottom-simulating-reflectors: calibration of the base of the hydrate stability field as used for heat flow estimates: Earth and Planetary Science Letters, v.109, p.289-301.

_____, and Spence, G.D., 1992, A seismic study of methane hydrate marine Bottom Simulating Reflectors: Journal of Geophysical Research, v.97, no.b5, p.6683-6698.

Kvenvolden, K.A., 1993, Subaquatic gas hydrate occurrence--models and settings: EOS, Transactions, American Geophysical Union, Supplement, v.74, p.369.

_____, and Barnard, L.A., 1983, Gas hydrates of the Blake Outer Ridge, Site 533, Deep Sea Drilling Project Leg 76: Initial Reports, DSDP, 76, p.353.

_____, and McDonald, T.J., 1985, Gas hydrates of the middle America Trench-Deep Sea Drilling Project Leg 84, in: von Huene, R., Aubouin, J., et al., Initial Reports, DSDP, 84, Washington (U.S. Govt. Printing Office). p.667-682.

_____, and McMenamin, M.A., 1980, Hydrates of natural gas: a review of their geologic occurrence: U.S. Geological Survey Circular 825, p.1-11.

Mackay, M.E., Jarrard, R.D., Westbrook, G.K., Hyndman, R.D., and the Shipboard Scientific Party of ODP Leg 146, 1994, Origin of Bottom Simulating Reflector: geophysical evidence from the cascadia accretionary prism: Geology, v.22, p.459-462.

Miller, J.J., Lee, M.W., and von Huene, R., 1991, An analysis of a seismic reflection from the base of a gas hydrate zone, offshore Peru: American Association of Petroleum Geologists Bulletin, v.75, p.2204-2213.

ODP Leg 146 Scientific Party, 1993, ODP Leg 146 examines fluid flow in Cascadia margin: EOS, Transactions, American Geophysical Union, Supplement, v.74, p.345.

Parsons, B., and Sclater, J.G., 1977, An analysis of the variation of ocean floor bathymetry and heat floor with age, Journal of Geophysical Research, v.82, no.5, p.803-827.

Reed, D.L., Lundberg, N., Liu, C.-S., McIntosh, K.D., Lieske, J.H. Jr., and Kuo, B.Y., 1991, Strain domains, fluid/gas migration and protothrusting in the offshore Taiwan accretionary wedge (abs.): Geological Society of America, Abstracts with Programs, v.23, p.365.

_____, Lundberg, N., Liu, C.-S., Kuo, B.-Y., 1992, Structural relations along the margin of the offshore Taiwan accretionary wedge: implications for accretion and crustal kinematics: Acta Geologica Taiwanica, no.30, p.105-122.

Rowe, M.M., and Gettrust, J.F., 1993, Fine structure of methane hydrate-bearing sediments on the Blake Outer Ridge as determined from deep-tow multichannel seismic data: Journal of Geophysical Research, v.98, no.b1, p.463-473.

Selly, R.C., 1983, Petroleum geology for geophysicists and engineers. International Human Resources Development Corporation, Boston, 87p.

Shipley, T.H., and Didyk, B.M., 1982, Occurrence of methane hydrates offshore southern Mexico: Initial Reports of the Deep Sea Drilling Project, v.66, p.547-555.

_____, Houston, M.H., Buffler, R.T., Shaub, F.J., McMillen, K.J., Ladd, J.W., and Worzel, J.L, 1979, Seismic evidence for widespread possible gas hydrate horizons on continental slopes and rises: American Association of Petroleum Geologists Bulletin, v.63, p.2204-2213.

Stein, C.A., and Abbott, D.H., 1991, Implications of estimated and measured thermal conductivity for oceanic heat flow studies: Marine Geophysical Researches, v.13, p.311-329.

Singh, S.C., Ninshull, T.A., and Spence, G.D., 1993, Velocity structure of a gas hydrate reflector: Science, v.260, p.204-207.

Suppe, J., 1981, Mechanics of mountain building and metamorphism in Taiwan: Memoirs of the Geological Society of China, p.67-89.

_____, 1984, Kinematics of arc-continent collision, flipping of subduction, and back-arc spreading near Taiwan: Memoirs of the Geological Society of China, p.21-33.

Tayor, B , and Hayes, D.E., 1983, Origin and history of the South China Basin. In: D.E. Hayes (ed), The Tectonic and Geologic Evolution of Southeast Asian Seas and Islands, Part II., American Geophysical Union Monogr. Ser.,27, p.23-56.

Teng, L.S., 1990, Geotectonic evolution of late Cenozoic arc-continent collision in Taiwan: Tectonophysics, 183, p.57-76.

Tucholke, B.E., Byran, G.M., and Ewing, J.I., 1977, Gas-hydrate horizons detected in seismic-profiles data from the western Northern Atlantic: American Association of Petroleum Geologists Bulletin, v.61, p.698-707.

Yamano, M., Foucher, J.-P., Kinoshita, M., Fisher, A., Hydman, R.D., and ODP Leg 131 Shipboard Scientific Party, 1992, Heat flow and fluid flow regime in the western Nankai accretionary prism: Earth and Planetary Science Letters, v.109, p.451-462.

Zwart,G., and Moore, J.C., 1993, Variations in temperature gradient of the Oregon accretionary prism: EOS, Transactions, American Geophysical Union, Supplement, v.74, p.222.